

# CHEMISTRY

## A European Journal



### Accepted Article

**Title:** Stereochemistry controlled supramolecular architectures of novel tetrahydroxy functionalized amphiphilic carbocyanine dye

**Authors:** Boris Schade, Abhishek Singh, Virginia Wycisk, Jose Luis Cuellar-Camacho, Hans v. Berlepsch, Rainer Haag, and Christoph Böttcher

This manuscript has been accepted after peer review and appears as an Accepted Article online prior to editing, proofing, and formal publication of the final Version of Record (VoR). This work is currently citable by using the Digital Object Identifier (DOI) given below. The VoR will be published online in Early View as soon as possible and may be different to this Accepted Article as a result of editing. Readers should obtain the VoR from the journal website shown below when it is published to ensure accuracy of information. The authors are responsible for the content of this Accepted Article.

**To be cited as:** *Chem. Eur. J.* 10.1002/chem.201905745

**Link to VoR:** <http://dx.doi.org/10.1002/chem.201905745>

Supported by  
**ACES**

WILEY-VCH

# Stereochemistry controlled supramolecular architectures of novel tetrahydroxy functionalized amphiphilic carbocyanine dyes

Boris Schade<sup>†,1</sup>, Abhishek Kumar Singh<sup>†\*,2</sup>, Virginia Wycisk<sup>2</sup>, Jose Luis Cuellar-Camacho<sup>2</sup>, Hans v. Berlepsch<sup>1</sup>, Rainer Haag<sup>2</sup> and Christoph Böttcher<sup>\*1</sup>

## I. Abstract

The synthesis of novel amphiphilic 5,5',6,6'-tetrachlorobenzimidacarbocyanine (TBC) dye derivatives with amino-propanediol head groups is reported, which only differ in stereochemistry (chiral enantiomers, meso-form, and conformer). For the achiral meso-form, a new synthetic route towards asymmetric cyanine dyes was established. All compounds form J-aggregates in water whose optical properties were characterized by spectroscopic methods. The supramolecular structure of the aggregates was investigated by cryo-transmission electron microscopy (cryo-TEM), cryo-electron tomography (cryo-ET), and atomic force microscopy (AFM) revealing extended sheet-like aggregates for the chiral enantiomers and nanotubes for the mesomer, respectively, while the conformer forms predominately needle-like crystals. The experiments demonstrate that the aggregation behavior of compounds can be controlled solely by head group stereochemistry which in case of the enantiomers enables formation of extended hydrogen bond chains by the hydroxyl functionalities. In case of the achiral meso-form, however, such chains turned out to be sterically excluded.

## II. Introduction

Cyanine dyes represent a class of organic dyes that are able to self-assemble in polar solvents and on solid surfaces.<sup>[1]</sup> Strong dipole-dipole coupling between the dye monomers leads to an electronically excited state shared by several monomers. Such exciton states cause a dramatic change in optical properties of the dye assemblies as compared to the isolated molecules.<sup>[2]</sup> Depending on the relative orientation between neighbouring monomers, different types of assemblies can be observed. A so-called "head-to-tail" configuration of transition dipoles leads to a red-shifted absorption band with large absorption cross section and superradiance.<sup>[2]</sup> Such assemblies are called J- or Scheibe-aggregates, named after their discoverers E. E. Jelly<sup>[1a]</sup> and G. Scheibe.<sup>[1b]</sup> The exceptional optical characteristics make J-

<sup>1</sup> Forschungszentrum für Elektronenmikroskopie und Gerätezentrum BioSupraMol, Institut für Chemie und Biochemie, Freie Universität Berlin, Fabeckstraße 36a, 14195 Berlin, Germany

<sup>2</sup> Institut für Chemie und Biochemie, Organische Chemie, Freie Universität Berlin, Takustrasse 3, 14195 Berlin, Germany

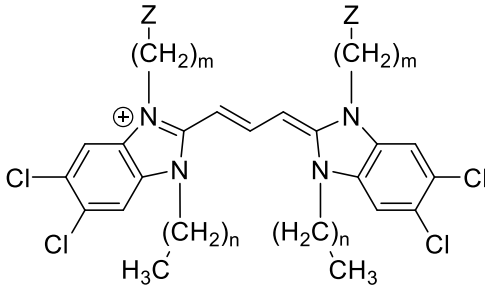
<sup>†</sup> These authors contributed equally to this work

aggregates interesting tools for a lot of applications ranging from dye-sensitized silver halide photography, light harvesting, photovoltaics, sensing, to biomedical imaging.<sup>[3]</sup>

Aggregation in polar solvents is a common feature of dye molecules containing extended planar  $\pi$ -electron systems. Further competing non-covalent interactions such as hydrogen bonding, halogen bonding or solvophobic forces support the aggregation and control the formation of complex supramolecular structures. Since dipole-dipole coupling strength and thus photophysical properties of the aggregates are highly sensitive to the particular arrangement of the chromophores, controlled structuring of dye assemblies by tuning supramolecular interactions between individual building blocks facilitates the design of novel materials with desired properties. Powerful approaches in this regard are specific alterations of the chromophore side groups, incorporation of additives, or modifications of the solvent polarity. In this context a class of derivatives of the well-known 5,5',6,6'-tetrachlorobenzimidacarbocyanine chromophore (TBC)<sup>[4]</sup> has been investigated in detail by several groups.<sup>[5]</sup> The chromophore was functionalized by attaching different polar or nonpolar substituents at the nitrogen atoms in 1,1' and 3,3' position. This allows for the tailored design of a large variety of supramolecular structures with interesting optical characteristics. By introducing 1,1'-dioctyl substituents, Dähne and co-workers advanced a class of amphiphilic dyes.<sup>[5a]</sup>

A fundamental prerequisite for studying dye assemblies is the availability of appropriate characterization methods. Cryogenic transmission electron microscopy (cryo-TEM) turned out to be an excellent technique to elucidate their morphology in the native environment of the solvent on the nanometre to micrometre scale.<sup>[6]</sup> Depending on the substituents of the TBC-chromophore one-dimensional fibres, two-dimensionally extended sheet-like aggregates, and single- or multi-layered tubular architectures with a helical molecular organisation were detected. The latter became a matter of particular interest as shape and size of such tubular aggregates resemble the natural light-harvesting system in green sulphur bacteria.<sup>[7]</sup> Thorough optical characterizations by linear optical spectroscopy, usefully supplemented by nonlinear techniques<sup>[8]</sup> or theoretical structure modelling<sup>[5e,9]</sup> are mandatory for a prospective use of photophysical characteristics. Although understanding of dye assemblies has made excellent progress over the last years, a substantial challenge remains: how does a particular molecular modification control the morphological and thus optical characteristics of the final supramolecular structure? So far, empirical approaches are still necessary due to a missing conclusive concept.

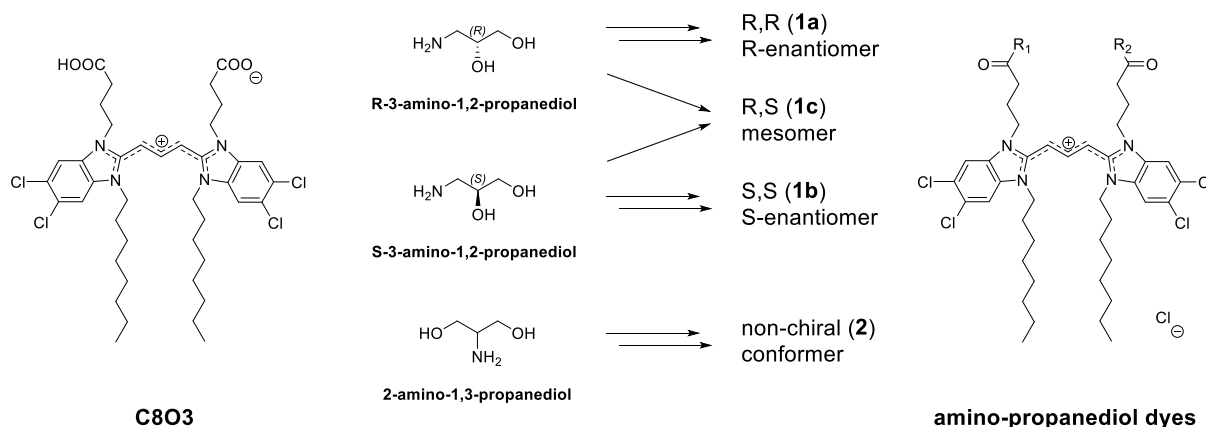
Table 1: Abbreviations for TBC based dyes



	Z	n	m
<b>TDBC (C2O4)</b>	-SO <sub>3</sub>	1	4
<b>C8S3</b>	-SO <sub>3</sub>	7	3
<b>C8O3</b>	-COOH	7	3

The most extensively investigated representatives of tube forming TBC based cyanine dyes are amphiphilic C8O3 bearing two carboxylic acid groups and C8S3 bearing two sulfonic acid groups.<sup>[5a, 10]</sup> (For abbreviations of TBC based dyes see Table 1) In aqueous media they are converted into their conjugate bases yielding negatively charged aggregate surfaces. Moreover, previous studies had revealed that the helicity of C8O3 tubes could be tuned upon addition of chiral alcohols.<sup>[11]</sup>

The goal of the present study was to prevent surface charge effects and to investigate the impact of chiral head groups on the supramolecular architecture of assemblies.



Scheme 1: Chemical structure of parent dye C8O3 and the family of newly synthesized amino-propanediol isomers.

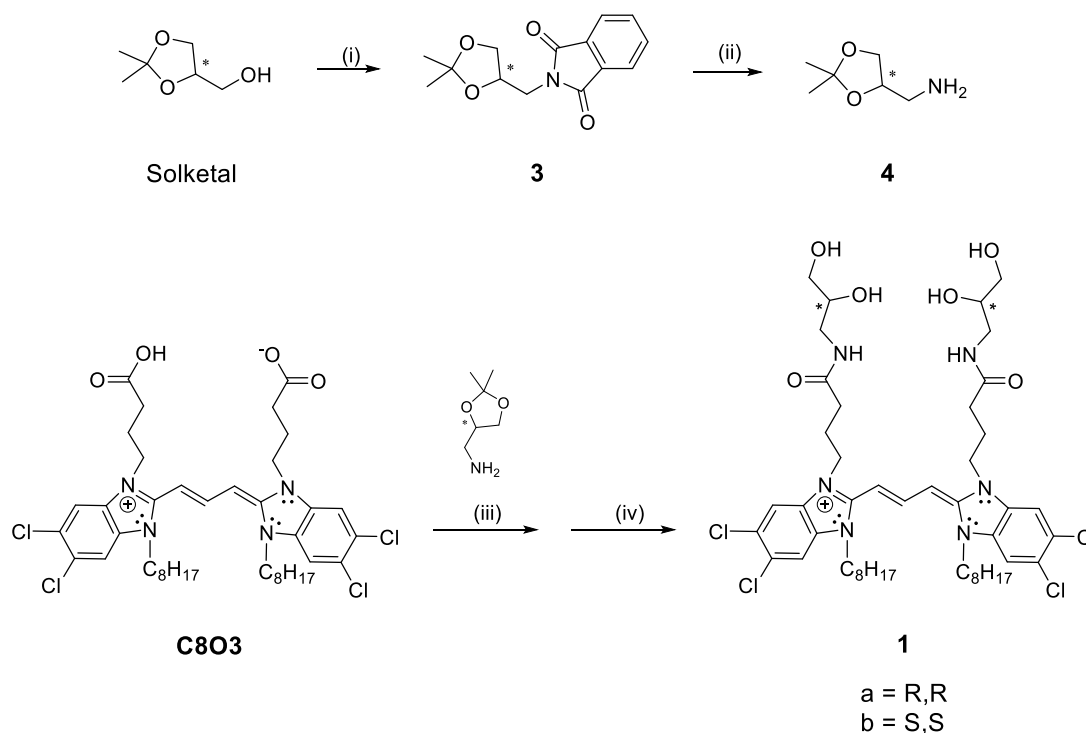
To achieve this goal, we selected C8O3 as parent TBC-derivative and functionalized both its carboxyl groups with amino-propanediol which provided a well-balanced amphiphilic character to allow for the formation of aggregates. Since there exist two conformations of amino-propanediol, chiral 1-amino-2,3-propanediol and non-chiral 2-amino-1,3-propanediol,

amidation of the two symmetrically situated carboxyl groups in C8O3 renders the formation of four different isomers possible, i.e., two enantiomers with either R,R or S,S configuration, a meso-form with R,S configuration and the non-chiral conformer derived from 1-amino-2,3-propanediol (Scheme 1). Hence, our approach allowed for versatile molecular alterations while the hydrophilic-lipophilic-balance (HLB) of the dyes and the spatial demand of the head groups remain unchanged. Moreover, it enables studies on the impact of the molecular chirality. With this structural diversity, we were able to elucidate the specific influence of head group stereochemistry and/or conformation on the aggregation behaviour of the novel amphiphilic cyanine dyes.

The studies of the C8O3 and C8S3 derivatives were used as guidelines for the present investigations and provided the basis for comparisons. The new derivatives were first characterized as monomers in organic solvents by absorption and fluorescence spectroscopy. Subsequently, aggregation in pure water was followed by absorption-, circular dichroism (CD), linear dichroism (LD), and fluorescence spectroscopy and structurally monitored by cryo-TEM, cryogenic electron tomography (cryo-ET) and atomic force microscopy (AFM). Structure models are presented and discussed.

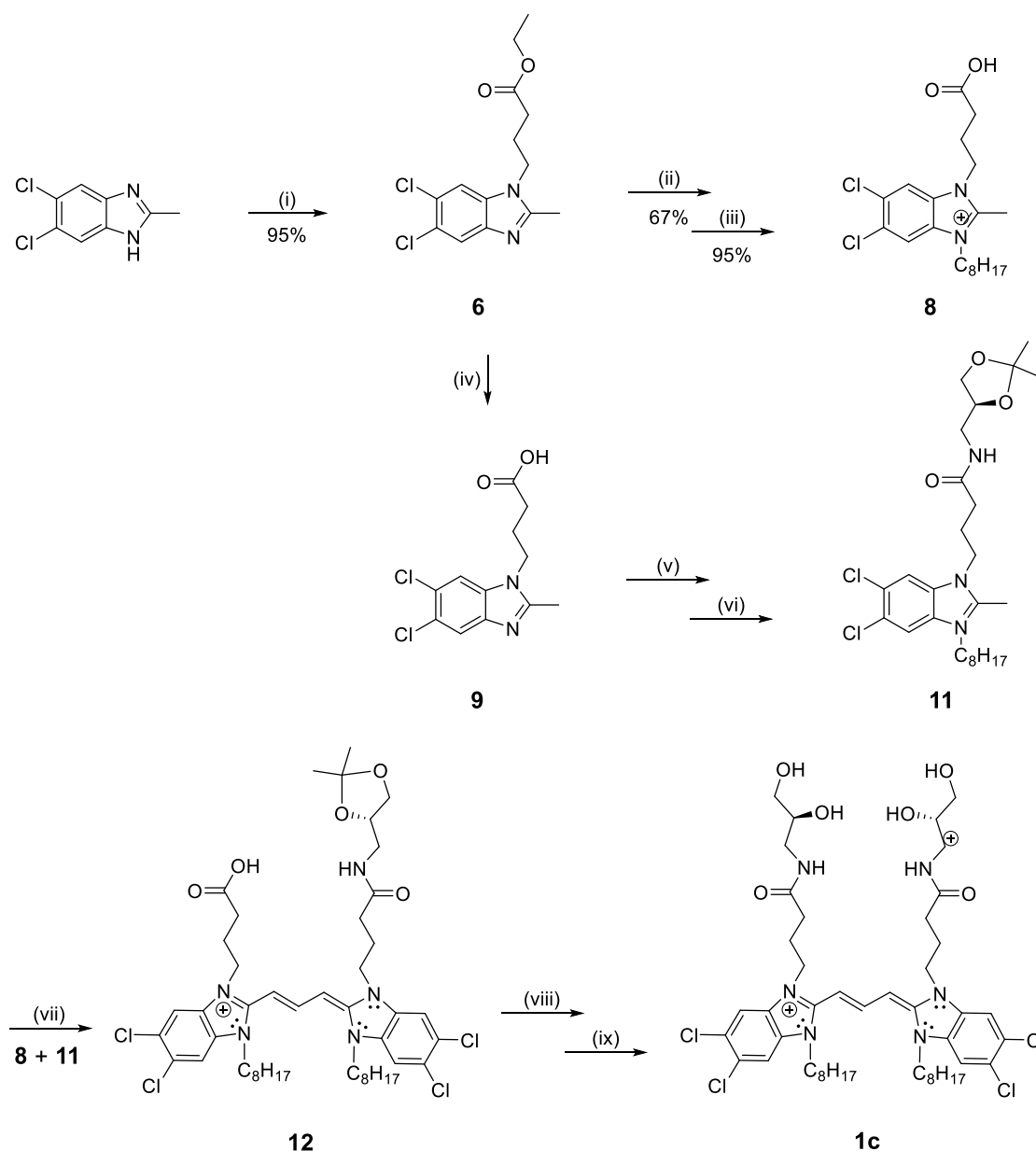
### III. Results and Discussion

#### Synthesis



Scheme 2: Synthesis of cyanine dye tetrahydroxy derivatives. i) PPh<sub>3</sub>, phthalimide, DEAD, THF, r.t., 20 h; ii) NH<sub>2</sub>-NH<sub>2</sub>, H<sub>2</sub>O, MeOH, reflux, 4-5 h; iii) HATU, DIPEA, DMF, r.t., 2 h; iv) HCl, MeOH, r.t., 2-5 h.

Synthesis of amino-propanediol cyanine dyes (compounds **1a**, **1b**, **1c** and **2**) has been achieved by two different synthetic approaches. A straight forward synthetic route was followed to obtain the isomers with uniform head groups, i.e. the R,R or S,S enantiomer from 3-amino-1,2-propanediol (Scheme 2), and the non-chiral symmetric serinol derivative (Scheme SI 4). To achieve and preserve the desired stereo chemistry and conformation of the chiral head groups, commercially available enantiopure solketal, i.e. the acetal of 1,2,3-propane diol, was chosen as starting material. This solketal (R or S) was converted into the respective solketal amine **4** in two steps (Scheme 2) and was then coupled to the acid groups of C8O3, followed by deprotection of the acetal groups under mild acidic conditions. The achiral serinol derivative **2** was synthesized accordingly using commercially available 2-amino-1,3-propanediol (serinol) without protection of the OH-groups following the same coupling procedure (Schemes SI 1-3).



Scheme 3: Synthesis of asymmetrical benzimidazoles; i) Ethyl-bromo acetate, NaOH, DMSO, r.t., 48 h; ii) 1-bromodecane, 150°C, 6 h; iii) HBr (48%), water, 120°C; iv) KOH, ethanol, reflux, 12 h; v) EDC.HCl, DMAP, DMF, 24 h, rt; vi) 1-bromodecane, 150°C; vii) DBU, CH<sub>3</sub>I, methanol, r.t., 48 h; viii) R-solketal, EDC.HCl, DMAP, DMF, 24 h, r.t.; ix) HCl, methanol.. (see the complete synthesis Scheme in SI)

Despite this convenient synthetic route above, a different strategy was necessary to synthesize the enantiopure meso-form (**1c**, Scheme 3). This mirror-symmetrical dye derivative was synthesized from two different monomers to attain its specific R,S conformation selectively. For that, 5,6-dichloro-2-methylbenzimidazole was subsequently treated with (i) ethyl 4-bromobutanoate and (ii) 1-bromo octane followed by hydrolysis in the presence of aq. HBr (iii) to yield benzimidazole **8**. The benzimidazole **11** was obtained by ester hydrolysis of **6** (iv), amidation with S-solketal amine (v), and finally N-alkylation with 1-bromo octane (Scheme 3).

Both benzimidazoles **8** and **11** were coupled in methanolic solution in the presence of DBU and CH<sub>3</sub>I. As expected, three different combinations of these two monomers led to the formation of three different dyes (Scheme SI 3). From their polarity order, however, it was possible to extract the desired cyanine dye **12** by performing column chromatography. Amidation with R-solketal amine and following acetal deprotection finally yielded the mesomer (**1c**).

### Spectroscopic characterization

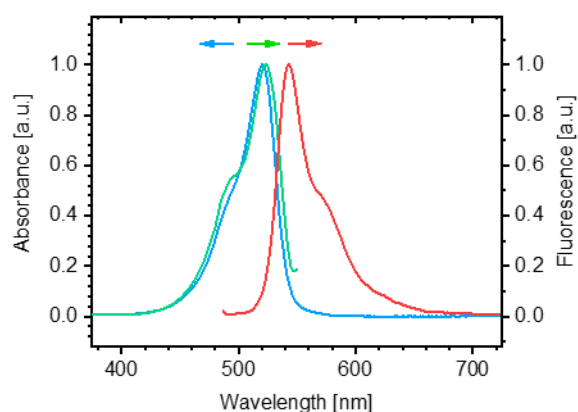


Figure 1: Normalized absorption (blue) and fluorescence spectra, excitation (green) and emission (red) of the new amino-propanediol R-enantiomer (**1a**) in methanol. The spectra are representative for all four compounds **1a-c** and **2**. Concentrations are 0.1 mM for UV and 0.01 mM for fluorescence measurements. The excitation spectrum was collected at 550 nm; the emission spectrum was collected after excitation at 480 nm.

The amino-propanediol dyes (**1a-c** and **2**) are readily soluble in MeOH and DMSO. In MeOH they all show an identical absorption band peaked at 520 nm (fwhm = 932 cm<sup>-1</sup>) with a vibronic shoulder at around 485 nm (see Fig. 1 for the R-enantiomer (**1a**)). The fluorescence emission spectrum reveals a mirror image of the absorption band with a maximum at 544 nm, yielding a Stokes-shift of 24 nm. The corresponding excitation spectrum resembles the absorption spectrum. The spectra are in good agreement with those of the parent derivative

C8O3, indicating that the introduction of the non-ionic amino-propanediol head groups with their particular chirality does not affect the spectroscopic properties of the chromophore. The spectroscopic features are typical for cyanine dye monomers.<sup>[12]</sup>

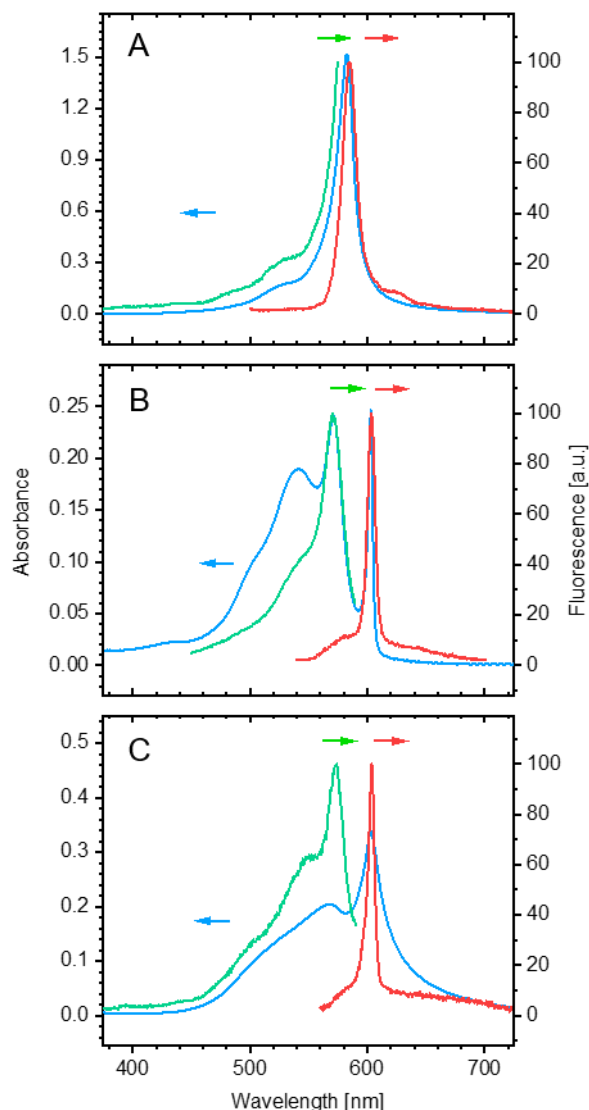


Figure 2: Absorption (blue) and fluorescence spectra, excitation (green) and emission (red) of (A) the R-enantiomer (**1a**), (B) the mesomer (**1c**), and (C) the conformer (**2**) in water, respectively. Matured stock solutions were diluted to concentrations of 0.1 mM for UV/vis and 0.01 mM for fluorescence on the verge of measurements. The fluorescence excitation spectra were collected at (A) 527 nm, (B) 604 nm, (C) 604 nm and the emission spectra were collected after excitation at (A) 488 nm, (B) 530 nm, (C) 550 nm, respectively.

The spectra of the dyes in water differ significantly from the monomer spectra in organic solvents (Fig. 2). Remarkable bathochromic shifts of the absorption band indicate the formation of J-aggregates<sup>[1c]</sup> in all cases (**1a-c**, **2**) and the influence of the compounds chirality becomes clearly visible by the differing absorption spectra of the enantiomers (**1a** and **1b**) and of the meso-form (**1c**).



Spectra of both enantiomers (**1a** and **1b**) are identical. The absorbance is characterized by a single narrow band at 583 nm ( $\text{fwhm} = 413 \text{ cm}^{-1}$ ) with a shoulder at 535 nm (shown exemplarily for the R-enantiomer (**1a**) in Fig. 2A). The fluorescence emission has its maximum at 585 nm. This nearly resonant emission is another typical feature of J-aggregates.<sup>[1c]</sup> The related excitation spectrum is in good agreement with the absorption spectrum. With respect to their shape all these spectra are similar to those found for the J-aggregates of the closely related cyanine dyes TDBC (C2S4)<sup>[5b]</sup> and C8O4.<sup>[13]</sup>

In contrast, the mesomer (**1c**) shows a split absorption spectrum (Fig. 2B) with a sharp and intense sub-band at 603 nm ( $\text{fwhm} = 165 \text{ cm}^{-1}$ ) and a second narrow and intense sub-band at 572 nm; a third broader band of lower intensity is located at around 543 nm. The emission spectrum shows only one sharp peak in resonance with the absorption band at 603 nm ( $\text{fwhm} = 247 \text{ cm}^{-1}$ ) regardless of the excitation wavelength.

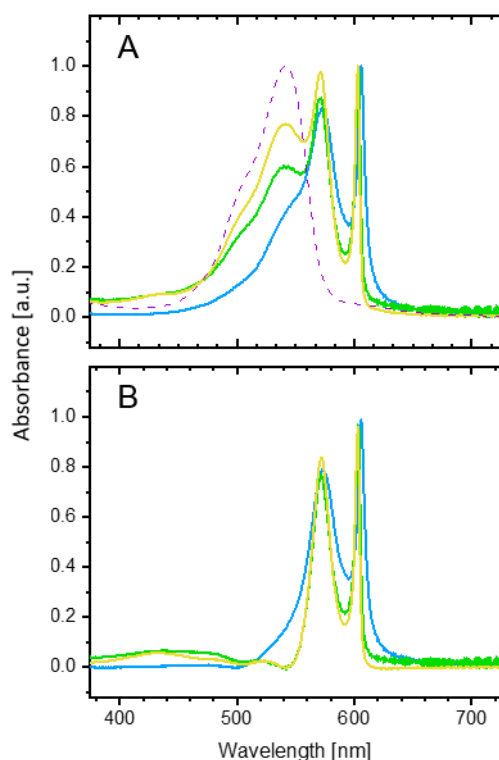


Figure 3: Three individual preparations from three different batches of the mesomer (**1c**) in Milli-Q water (yellow, green and blue) show a differently strong third sub-band at  $\sim 543 \text{ nm}$ , while the two longer-wavelength bands remain almost stable (A). The individual spectra are normalized to the same absorbance at  $\sim 603 \text{ nm}$ . The dotted spectrum was derived from a solution of **1c** in HCl at a  $\text{pH} < 4$ . After appropriate scaling and subtraction of this low pH spectrum from the three spectra in Milli-Q water, two-banded spectra are obtained for all preparations as shown in the lower panel (B).

Fig. 3A shows a family of spectra from three individual mesomer (**1c**) sample preparations. The comparison reveals differences in the intensity of the third absorption band at 543 nm, which clearly exceed the experimental error limits. Also, the maximum position of the longest

wavelength band varies slightly from sample to sample but to a much lesser extent (between 603 and 606 nm). It is noticeable, however, that the intensity ratio of the first and second sub-band remains almost constant. When the mesomer was dissolved in aqueous HCl at low pH (lower than 4) the solution displays a spectrum with a maximum at 543 nm (purple dotted line), which resembles that of monomers (Fig. 1), but is clearly broader (fwhm = 1295  $\text{cm}^{-1}$ ) and red shifted by about 23 nm. After appropriate scaling and subtraction of this band from the spectra in Milli-Q water (Fig. 3A), roughly identical, two-banded spectra are obtained for all three preparations (Fig. 3B). This simple fit procedure suggests that the remaining longer-wavelength bands belong to the aggregate while the variable third band around 543 nm might indicate the presence of a further independent species (probably dimers or smaller oligomers).

The conformer (**2**) displays a split absorption spectrum in water (Fig. 2C, blue) just as described for the mesomer (**1c**). In case of the conformer (**2**), the bands became broader and their intensity weaker within a period of minutes indicating precipitation. The fluorescence behaviour, however, is similar to the mesomer. Due to the rapid precipitation the conformer was not investigated in more detail by spectroscopy.

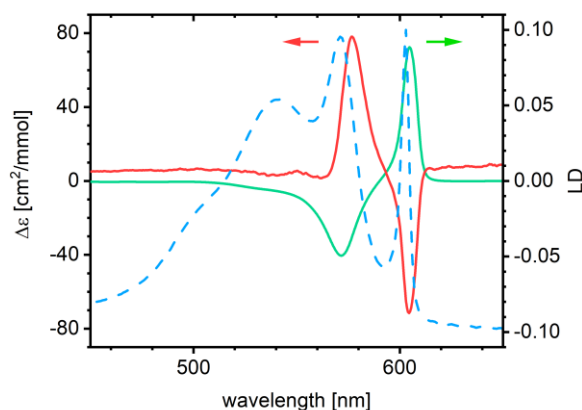


Figure 4: Circular (red line) and linear dichroism (green line) spectra of an aqueous solution of achiral mesomer (**1c**). To compare the peak positions, a normalized isotropic absorption spectrum (blue broken line) is added to the graph without a dedicated ordinate.

In former studies we demonstrated that the achiral parent dye C8O3 forms optically active helical J-aggregates by applying circular dichroism (CD) spectroscopy and cryo-TEM. Moreover, we were able to tune the handedness of aggregates by adding chiral alcohols.<sup>[10a, 11]</sup> Therefore, we were interested to see whether the use of chiral head groups affects the supramolecular assembly in a similar way. The absence of CD signals from methanolic solutions of the dyes indicates that the chirality of head groups has at the best negligible effect on the conformation of the monomeric (non-aggregated) chromophores.<sup>[14]</sup> In contrast, the aggregated mesomer (**1c**) shows negative and positive Cotton effects at 577 and 605 nm, respectively (Fig. 4, red line). Phenomenological, this behaviour is in line with corresponding

CD results of the parent C8O3 dye and points to a similar molecular architecture of aggregates. For this dye a tubular architecture was detected, with the tube wall being composed of two helically twisted chromophore layers.<sup>[5b]</sup> The observed Cotton effects were ascribed to molecular excitons. In the case of the related C8S3 dye the helical architecture of tubes was even proven directly by highly resolved cryo-TEM images.<sup>[6, 15]</sup> For the enantiomers (**1a** and **1b**), however, we did not obtain spectra with mirror symmetry, indicating the absence of a chiral supramolecular organisation. Morphological investigations proved this claim (see below).

Linear dichroism (LD) spectroscopy is a highly sensitive method that can give valuable information about the molecule packing orientation within aggregates. Isotropically oriented molecules give no LD signal, while anisometric aggregates with high aspect ratio give characteristic LD signals. To measure the linear dichroism the aggregates dispersed in the sample have to be aligned.<sup>[16]</sup> For fibrous aggregates (cf. Fig. 8 and Fig. 9), this can simply be accomplished in the streaming field of a Couette flow cell. Solutions of the mesomer (**1c**) show a LD spectrum (Fig. 4, green line) consisting of two strong sub-bands, which locations coincide with the two strongest absorption bands. The positive LD signal of the longest-wavelength band (604 nm) indicates a parallel polarization of the associated transition with respect to the aggregates' long axis. The other band (571 nm) is polarized perpendicularly. This polarization pattern is characteristic for single-layered tubular J-aggregates.<sup>[5e, 17]</sup>

Analog LD measurements of the enantiomer solutions gave only one small positive band. This finding is difficult to interpret because the sheet-like structure of these aggregates (cf. Fig. 6 as evidence) casts serious doubts on their ability to be directionally oriented in the Couette cell.

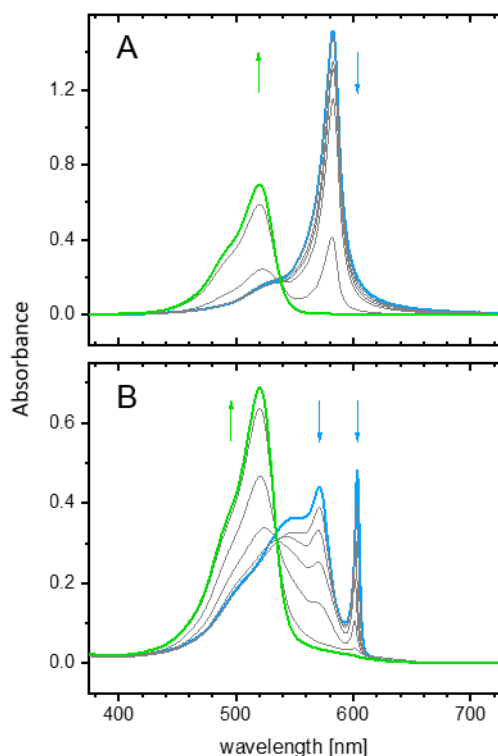


Figure 5: Disaggregation of J-aggregates of (A) the R-enantiomer (**1a**) and (B) the mesomer (**1c**) upon MeOH titration. The equilibration time between each titration step was 5 min. Start solution: 0.1 mM dye in pure water. Arrows indicate the effect of increasing MeOH concentration: (A): [MeOH]: 0, 10, 20, 30, 40, 50, and 60%; (B): [MeOH]: 0, 10, 20, 30, 40, 45, 50, and 60%.

Due to the solubility of dyes in methanol, disaggregation can simply be monitored by absorption spectroscopy upon methanol titration. Such measurements provide additional information about the stability of aggregates and the kinetics of disaggregation. In the experiments reported here, we added a methanolic dye solution to the respective aqueous solution of the aggregated dyes in order to keep the dye concentration constant.

Fig. 5 displays sets of absorption spectra for the R-enantiomer (**1a**, Fig. 5A) and the mesomer (**1c**, Fig. 5B). The absorbance of **1a** remains almost unchanged up to 30 vol% methanol admixture. Further admixture of up to 60 vol% promotes the gradual formation of monomers at the expense of J-aggregates. A defined isosbestic point at 540 nm indicates disassembly of J-aggregates directly into monomers without the appearance of intermediates.

A slightly different result was obtained for the mesomer (Fig. 5B). Here, the isosbestic point is located at 535 nm. In contrast to the R-enantiomer, the J-bands remain almost unchanged up to 20 vol% of methanol. Complete disassembly of the aggregates is accomplished at 50 vol%. Noticeable is the appearance of a hump at around 540 nm prior to complete disassembly. By deconvolution of the spectra into monomer and aggregate components (not shown) a corresponding band could indeed be extracted, but an associated aggregate species could not be detected by cryo-TEM.

### Structural Characterization

Spectroscopic investigations of all aqueous amino-propanediol dye solutions (**1a-c**, **2**) were complemented by direct structural characterisation using cryo-TEM, cryo-ET, as well as AFM imaging techniques.

#### Sheet-like assemblies for the enantiomers

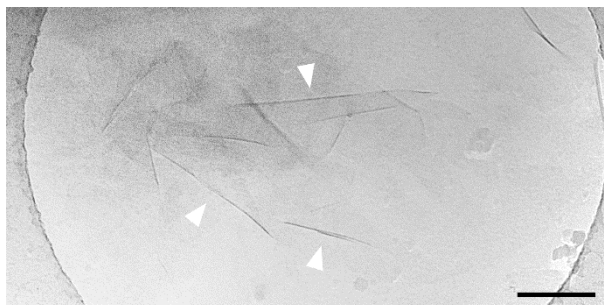


Figure 6 The cryo-TEM micrograph of a 0.1 mM solution of the R,R enantiomer **1a** in pure water discloses the formation of sheet-like aggregates. Their approximate thickness can be roughly estimated from wrinkles (arrow heads) measuring  $6 \pm 1$  nm. Bar represents 200 nm.

Both enantiomers (**1a** and **1b**) assemble into sheets with dimensions in the micrometre range (Fig. 6). The sheets are separated without any tendency to form stacks. Occasionally emerging wrinkles (dark lines marked by white arrow heads) were used to estimate a sheet thickness of approximately 6 nm. This value, however, is only a rough estimate due to inhomogeneous folding events and blurring at the edges of the folds.

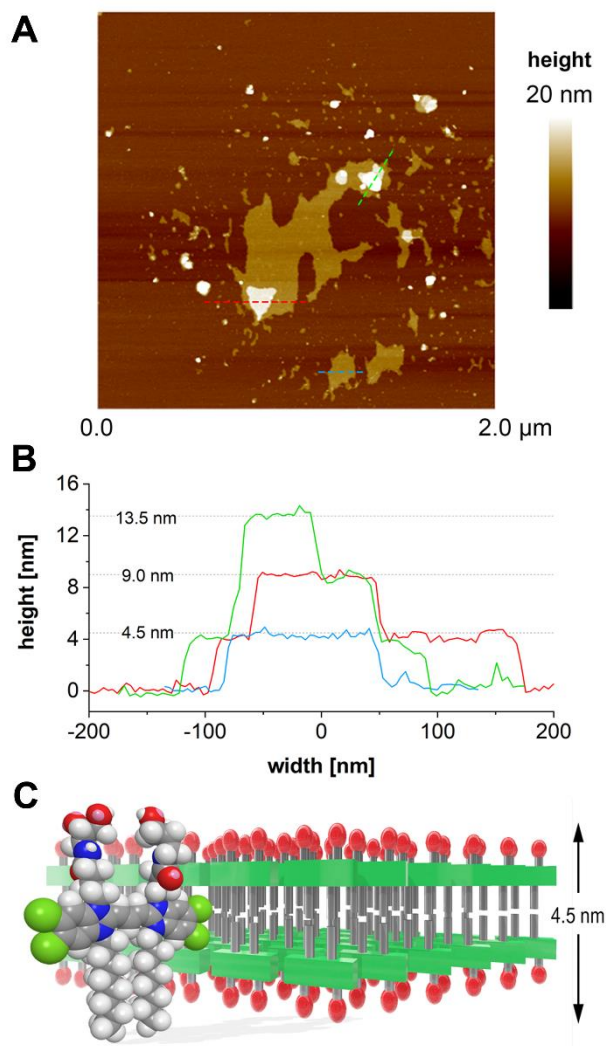


Figure 7: A) AFM reveals the deposition of the sheet-like aggregates from the R-enantiomer (**1a**) on mica. B) The height profiles measured along the trajectories depicted by dashed lines in the top view image show recurring 4.5 nm steps, even when smaller aggregates are deposited on top of the large sheets (red and green line). C) Space filling model of the amino-propanediol cyanine dye and a schematic representation of a J-type bilayer arrangement thereof. The model reproduces the distance between opposing chromophores and the overall thickness of the sheet-like aggregates from the enantiomers as elucidated by the AFM measurements. TBC chromophores in a brickwork arrangement are represented by green blocks, diol head groups by red ovals, and hydrocarbon chains by grey rods.

For a more accurate thickness determination, AFM measurements were exemplarily performed on R-enantiomer sheets deposited on mica support in a water-filled liquid chamber. Sheets with a thickness of 4 - 4.5 nm were imaged in *PeakForce* mode (Fig. 7A and B). Even smaller sheets deposited on top provided additional ~ 4.5 nm high plateaus. The value corresponds approximately to twice the length of the molecule and thus indicates a bilayer arrangement of dye molecules (Fig. 7C). Despite a high level of order as suggested by the narrow absorption band (cf. Fig. 2), ultra-structuring of the sheets' surface could not yet be resolved.

### Tubular assemblies of the mesomer

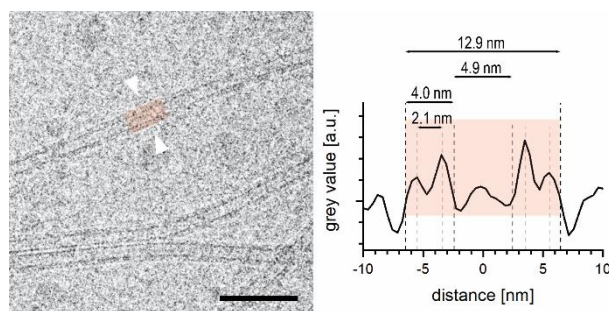


Figure 8 Left: The cryo-TEM micrograph of a two days old 1 mM solution of the mesomer (**1c**) in pure water displays uniform individual tubes. Their length often exceeds several micrometres. The line plot (right) across the highlighted tube section provides the cross-sectional density and thus allows for the precise characterization of the tubes' double layer structure and its dimensions. Bar represents 50 nm.

Other than the enantiomers, the mesomer (**1c**) forms tubular supramolecular aggregates. In one particular preparation we found almost exclusively individual tubes with maximum lengths reaching several micrometres, while other preparations predominantly showed tube bundles with varying degrees of twist. Once formed, the particular proportions of tubes and bundles in either sample persisted over the time (Fig. SI 2). The heterogeneity in preparation-dependant structural varieties, however, remains unexplained.

Fig. 8 displays a sample of **1c** in which almost exclusively individual tubes were formed. The high spatial image resolution discloses the double layer architecture of the tube walls. The line plot (right) averages the grey values of a 41 nm long straight tube section (red area) along its central axis and thus provides the tubes' cross-sectional electron density with enhanced signal-to-noise ratio. The labelled tube has an outer diameter of  $\sim 12.9$  nm and an inner diameter of  $\sim 4.9$  nm. The total thickness of the wall is about 4.0 nm (dark dashed lines) and the peak to peak distance (highest densities) between the layers measures 2.1 nm (light dashed lines) and corresponds to previous data of C8O3 tubes.<sup>[5b, 18]</sup> The peaks mark the positions of the electron rich dye skeleton (chromophore). Thus, the profile of the bent double layer of the tubes is in good agreement with that of the flat double layer (cf. Fig. 7C) and matches the molecular dimensions.

To look for long-time changes of the morphology we re-examined the 1 mM solution after 2, 21, and 125 days. The statistical analysis of in total 344 line plots as in Fig. 8, i.e. approximately 100 from each sample, yielded mean diameters of 12.7, 12.5, and 12.7 nm, respectively, with standard deviations of 0.76, 0.97, and 0.64 nm for each subset. This proves a robust geometry of the individual tubes even upon long-time storage.

The (outer) tube diameter is a little larger than for the parent dye C8O3 (for pure dye:  $\sim 10.0$  nm<sup>[5b]</sup>, for PVA stabilized tubes: 11.5 nm<sup>[18]</sup>) and comparable with that of the sulfonic acid



analogue C8S3 prepared by the alcoholic route (13 nm<sup>[9a, 19]</sup>). The wall thickness of about 4 nm, however, is almost identical for all tubes.

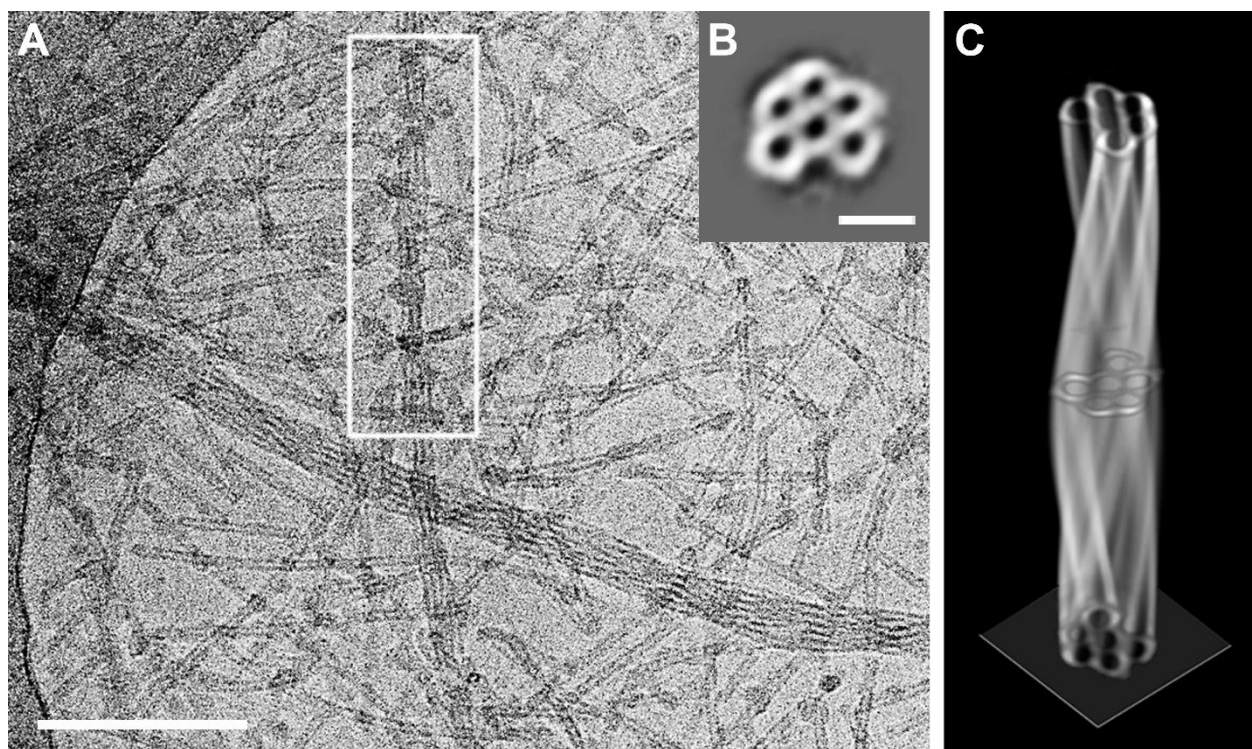


Figure 9 (A) Cryo-TEM micrograph of mesomer (**1c**) in 1mM aqueous solution which was subjected to cryo-ET showing individual tubes and twisted tube bundles. Bar represents 200 nm. (B) A sum-image of aligned slices extracted perpendicular to the long axis of the labelled bundle from the reconstructed volume provides the mean cross-sectional density with enhanced signal-to-noise ratio (note the inverted contrast necessary for image processing). Due to the rotation of the motif upon following the bundles' long axis the missing wedge artefact of the tomography reconstruction can be overcome. Bar represents 50 nm (C) The averaged cross-section was used to reconstruct a 3D-model of the bundle which is presented in voltex<sup>[20]</sup> representation to illustrate the twisted course of the constituting tubes.

Fig. 9A displays a cryo-TEM micrograph of a 1 mM solution of the mesomer (**1c**). Here, next to short individual tubes also tube bundles such as often found for the parent dyes C8O3<sup>[5b, 21]</sup> and C8S3<sup>[5e, 19]</sup> are obtained.

To elucidate the three-dimensional volume structure of the twisted bundles, we subjected the sample to cryo-ET. The tomogram was reconstructed from 65 single exposures taken at angles from  $-65^{\circ}$  to  $63^{\circ}$  in two-degree tilt increments. Slices of the tomogram along the boxed bundle (Fig. 9A) provide 5 tubes which are hexagonally arranged around a sixth central tube (B). This composition leaves a void at the outer face of the aggregate which permits to follow the continuous displacement of this pattern along the bundle long axis by scrolling through the slices of the tomogram (see Fig. SI 4). A complete 360° cycle corresponding to the bundles' pitch is 400 nm. 232 extracted slices were used to calculate the mean cross-section of the bundle with enhanced signal-to-noise ratio (B). Due to the complete 360° rotation of the motif



along the bundle long-axis a complete and accurate density profile is averaged without restriction of the missing wedge artefact. This motif was used for the reconstruction of the complete volume of the bundle (Fig. 9C). It becomes apparent that the wall thickness between the tubes and towards the exterior of the bundle is the same, disclosing that the tube walls double-layer construction is absent in the interior of the bundles, where tubes should form two double-layers at their contact faces.

Recently, Eisele *et al.*<sup>[5e]</sup> elucidated the same tube layer deviation for bundles of C8S3 by using cryo-ET volume reconstructions. They assumed that upon bundling the originally bilayered tubes lose their outer layer. In the following we describe an image-based approach to reveal an even more detailed insight into this unusual molecular tube layer organisation.

### Modelling of tube bundles

Due to the limited resolution in cryo-ET data, more detailed information about the supramolecular construction can be obtained by analysing individual cryo-TEM projection images recorded at higher magnification by a geometry-based simulation approach. We were in particular interested in the structural organization at the interfaces of adjacent tubes. Hereby, the hexagonal arrangement of tubes as observed by cryo-ET (cf. Fig. 9B) provided the basic motif.

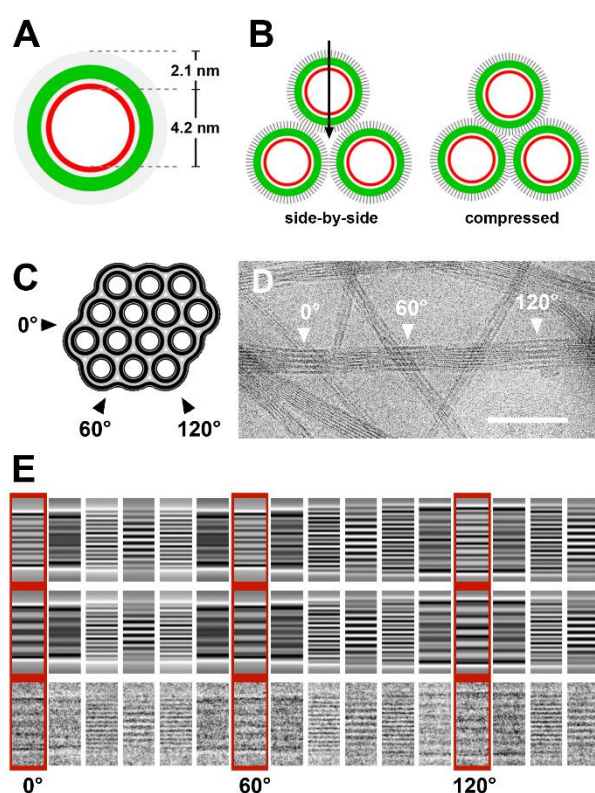


Figure 10: Modelling of a twisted tube bundle. (A) Cross-sectional view of a model tube with a mono layered wall. Constituting dye molecules are oriented with their head groups (red) towards a central channel whereas octyl chains (grey) point outwards. (B) Packing motifs for the tubes in a bundle.

*Side-by-side* arrangement of the tubes (left) leaving voids at the interfaces. *Compressed* packing of the tubes (right) diminishes interspaces. (C) Cross-section of a bundle of mono layered tubes (cf. A) reproducing the number and orientation of the tubes in the original bundle in (D). This cross-section was used to generate a 3D model of the respective bundle (cf. Fig. SI 6). (D) Cryo-TEM image of twisted bundle with the marked positions of characteristic line patterns. (E) Back projection patterns in  $10^\circ$  steps of 3D models calculated for the side-by-side arrangement (row 1), the compressed packing (row 2) and the experimental cryo-TEM data (row 3). Projection images of the *compressed* arrangement reveal a much better match with the experimental data.

The projection pattern along the twisted bundle in Fig. 10D was used as experimental reference. As the changes in the pattern along the bundle axis are a structural equivalent for a rotation around the bundle axis (as proven by the cryo-ET data), we compared the systematic variation in the experimental projection pattern with that of a rotated hexagonally packed bundle of tubes, whose multiplicity and tube diameter can be determined directly from the cryo-TEM image (cf. Fig. SI 5). For the case at hand (see Fig. 10D), we determined multiplicities of 4, 4, and 5, layers in the directions of  $0^\circ$ ,  $60^\circ$ , and  $120^\circ$ , respectively, and a tube diameter of 8.4 nm from the line distances at  $30^\circ$ ,  $90^\circ$ , or  $150^\circ$ . These values indicate a tube arrangement as shown in Fig. 10C.

We calculated the back-projections of the respective 3D-volume and compared them with the experimental data. The back-projection patterns of the side-by-side arranged tube bundle (Fig. 10E, row 1) coincide fairly well with the data. A compressed (interdigitated) arrangement of the monolayered tubes (Fig. 10B, right), however revealed a much better fit (Fig. 10E, row 2). Moreover, in this arrangement the unfavourable voids at the trigonal contact interfaces of the tubes (arrow in Fig. 10B, left) are largely diminished (right).

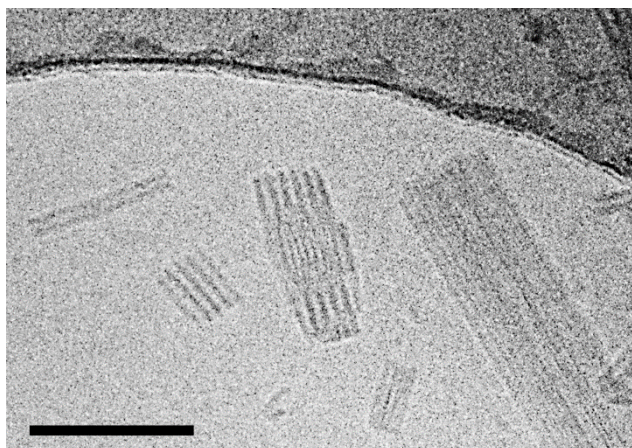


Figure 11 Twisting and bundling starts at the early state of the aggregation process. This micrograph shows a vitrified sample prepared six hours after the dissolution of the solid matter in water. Next to short individual tubes a short ( $\sim 100$  nm length) twisted bundle can be found. Bar represents 100 nm.

To obtain information about the assembly process of the tube bundles we prepared early states of aggregation. A cryo-preparation 6 hours after dissolution of the dye shows short only 50 - 100 nm long bundles (Fig. 11) which already exhibit the typical patterns of a twisted bundle (cf. Fig. 9). Its existence at this early stage of the aggregation process as well as the

persistence of individual tubes indicates a new aspect of the assembly growth, i.e. the hierarchical organization of tubes into bundles obviously results from intrinsic supramolecular interactions at the start of aggregation and contravenes the assumption that bundling and twisting is caused in a multi-stage process over time.

#### *Needle-shaped crystals of the conformer*

Conformer (**2**) showed macroscopically visible needle like aggregates, too large to be preparable for cryo-TEM. Upon addition of methanol, however, needles became significantly smaller and thus enabled cryo-TEM investigations.

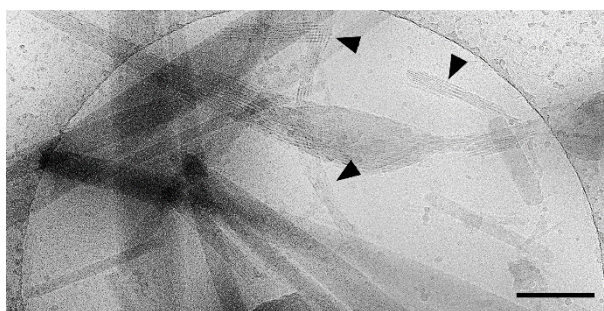


Figure 12 Cryo-TEM micrograph of an aqueous solution of the conformer (**2**) containing 30 vol% of methanol displaying a few tube bundles (black arrow heads) and predominantly wide elongated and non-twisted crystalline assemblies. Bar represents 100 nm.

In contrast to the mesomer (**1c**) cryo-TEM micrographs of aqueous solutions of the conformer (**2**) revealed only very few individual tubes or tube bundles (Fig. 12, black arrowheads), while predominantly formation of smooth elongated structures occurs. The latter can reach lengths of several micrometres and widths of hundreds of nanometres. Despite their dimension, the large assemblies seem to preserve some flexibility as many of them are slightly bent. Nevertheless, frequently occurring very narrow line patterns suggest a repetitive crystalline order. These morphological findings are in line with the observed spontaneous precipitation of dye **2** and the remarkably broad absorption bands. Although tube-like aggregates were formed in negligible amounts, crystallization seems to dominate over supramolecular aggregation in case of the conformer (**2**).

#### *IV. Discussion*

Monomer spectra of all novel dyes coincide with the respective data of the parent dye C8O3 proving that the modifications in the head group chemistry have no effect on the electronic properties of the chromophore. In water red shifted absorption spectra indicate the formation of J-aggregates for all four dyes. Spectral differences among the new dyes as well as in relation to C8O3 or C8S3, which only differ in the hydrophilic head groups, indicate different molecular organizations.

The structural investigations showed that the enantiomers (**1a** and **1b**) form sheet-like aggregates as observed earlier for the related dyes TDBC (C2S4) and C8O4.<sup>[8]</sup> Absorbance and fluorescence spectra are quite similar and in line with the supramolecular structure of the aggregates. Brickwork-like arrangements of molecules in flat two-dimensionally extended sheets can explain this behaviour.<sup>[22]</sup> In contrast, spectra of the mesomer (**1c**) resemble those of special preparations of the reference dyes C8O3 and C8S3 where bundles of tubes dominate.

Isolated tubes show two longitudinally polarized transitions on the low-energy side of the absorption spectrum. Thereby, both transitions are radiative. In addition, perpendicularly polarized transitions are observed at higher energy. This results from the double layer architecture of the tube walls.<sup>[5f, 18, 23]</sup> In contrast, single-layered tubes show only one longitudinally polarized low-energy transition accompanied by a perpendicularly polarized transition at higher energy and only one emission band in resonance with the low-energy absorption band.<sup>[17]</sup> Eisele *et al.*<sup>[5e]</sup> explained this quite interesting effect by the loss of the outer dye monolayer during the bundling process. A similar spectral single-layer signature was observed for preparations of the mesomer (cf. Fig. 2B and Fig. 4). Since tube bundles were also detected for the mesomer (**1c**), we suggest the same mechanism being valid for this derivative. Volume reconstruction from cryo-ET data and modelling of highly resolved tube bundle projection images support this concept and add additional details. The observation of a spectral single-layer signature for the preparation with exclusively isolated double-layered tubes, however, cannot be explained at present.

The amphiphilic dye aggregation in water is driven by a multitude of different forces: amphiphilic and dispersive interactions of alkyl chains, chromophores, and the extended planar  $\pi$ -systems as well as interactions and steric demand of the head groups. Since both, the hydrophobic part of the molecules and the chemical composition of the head groups are identical for all the new dyes, the differing aggregation behaviour must result from differing interactions of the head groups due to their stereochemistry. Our results reveal, that inversion of one stereo centre (enantiomer *vs.* mesomer) induces the formation of completely different architectures, i.e. sheets (Fig. 6) and tubes (Fig. 8 and Fig. 9), respectively, associated with particular spectroscopic characteristics.

The chiral enantiomers (**1a** and **1b**) form planar, hence achiral aggregates, which is a rather unexpected result given the multitude of chiral ultra-structures reported for chiral compounds in literature. Thickness measurements indicate that the sheets of the enantiomers are formed by molecular double layers, as expected from the amphiphilic character of the dyes.

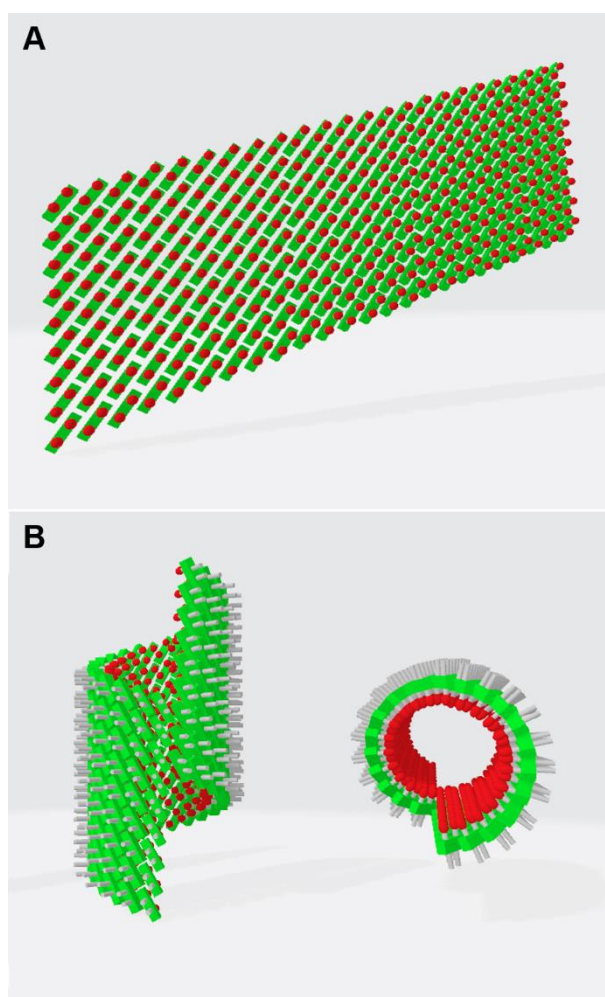


Figure 13: The brickwork arrangement of cyanine dyes constitutes the basic arrangement of the molecules in sheet-like J-aggregates (top). If rolled up into tubes (bottom) a helical arrangement of the constituent dyes results which causes a strong CD signal of the superficially achiral structure.

According to theory, the spectroscopic properties of J-aggregates can be explained by a so-called “head-to-tail” arrangement of the transition dipoles of the chromophores. Such an arrangement is realized in a two-dimensional layer of dye molecules, where neighbouring molecules are shifted against each other in a brickwork-like pattern (Fig.13A).<sup>[2, 22]</sup> The model explains the occurrence of a single sharp absorption band and the quasi-resonant emission. This simple spectroscopic behaviour is observed for many sheet-like J-aggregates including the related cyanine dyes TDBC (C2S4) and C8O4, which form extended monolayers and double-layered sheets, respectively.<sup>[5b]</sup> Considering their similar spectroscopic and structural features we assume a comparable brickwork arrangement for the enantiomers (Fig. 13).

The fact that the chiral enantiomers (**1a** and **1b**) form planar structures upon aggregation seems all the more surprising because the related achiral dyes C8O3 and C8S3 form double-layered tubular structures instead. Some of these tubular structures reveal even helical packing patterns<sup>[6, 15]</sup> and the tubes show generally a strong tendency to assemble into twisted rope-like bundles.<sup>[5b]</sup> Hence, such tubes possess a chiral structure and their absorption



behaviour can be modelled on this basis.<sup>[5f, 8c, 9a, 23]</sup> The ability of the presented non-chiral derivatives, i.e. the achiral mesomer (**1c**) and the non-chiral conformer (**2**), to form tubes suggests a comparable architecture. Considering the Cotton effect of their CD spectra (Fig. 4), at least the tubular assemblies of the achiral mesomer (**1c**) are organized in a chiral molecular arrangement (Fig. 13B).

The obvious inverse relationship between molecular chirality and helicity of supramolecular architecture asks for a model that can explain the various structures and is consistent with the detected spectra.

The formation of chiral supramolecular structures from achiral or non-chiral molecules in solution has been reported but remains rare.<sup>[24]</sup> This may derive from the even probabilities to form right- or left-handed assemblies resulting in a net zero CD-signal. Only homochirality can be detected unambiguously by CD spectroscopy. Examples include the non-chiral cyanine dye C8O3<sup>[10a, 11]</sup> or the generation [1.0] polyglycerol amphiphile reported by Kumar *et al.*<sup>[25]</sup> In the latter case, chiral ultra-structuring of the self-assembled tubes was detected by CD only in the case of the meso-form. The origin of this supramolecular chirality was explained to result from the cooperation of a fixed lateral arrangement of molecules and specific intermolecular hydrogen bonding patterns of the hydroxyl groups, which produces a strong helical twist of the molecular stacks only in case of the meso-form.

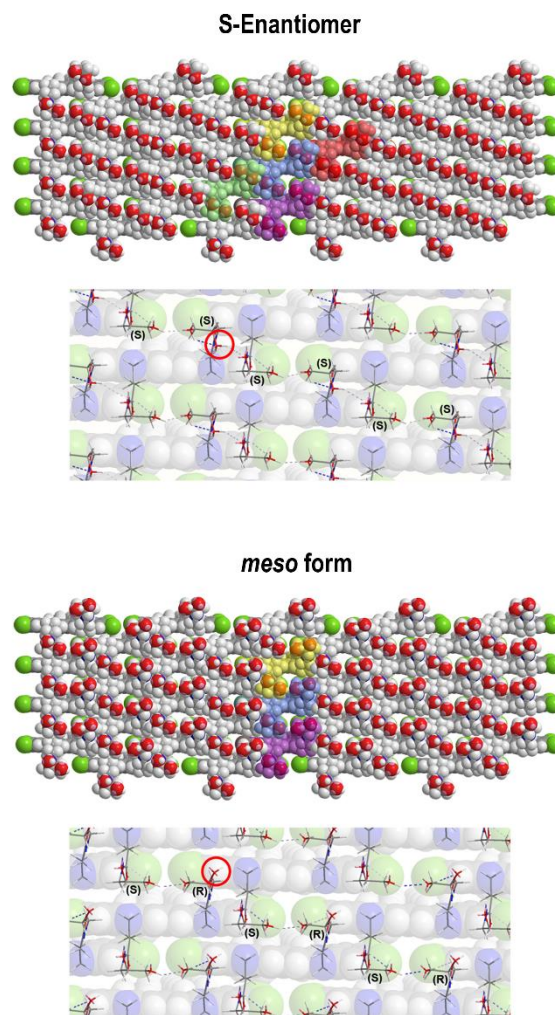


Figure 14 (Top) The brickwork arrangement of the S enantiomers gives rise to continuous strings of hydroxyl groups (red) running transversely to the chromophore skeletons (coloured in background). The close up (below) shows the OH groups properly situated to form endless hydrogen bridge chains. Hence, all dye molecules are connected to four neighbouring molecules (coloured). This stable two-dimensional arrangement is the unique feature for the chiral enantiomers and cannot be realised by the meso-form (bottom) due to the different orientation of the respective OH group at the chiral centre (red circles).

We consider a quite similar reason here. In a brickwork arrangement of the enantiomers forming the planar double-layer, the rows of molecules are positioned in a way that neighbouring rows are staggered approximately by half of the chromophore length (Fig. 14). The distance between the rows results from the space demand of the chromophore skeletons which is 0.35 – 0.4 nm. By placing the enantiomers accordingly, continuous strings of hydroxyl groups can be observed running transversely in respect of the rows of the chromophores (top left). A more detailed presentation (bottom left) shows that all OH groups within a row are connected by endless hydrogen bond chains. Thus, each dye molecule interacts strongly with four neighbouring molecules stabilizing the planar arrangement. In case of the mesomer, however, the inversion of one of the chiral centres prevents linear hydrogen bonds of hydroxyl groups due to their alternating orientation (marked by a red circle). The curved molecular

arrangement upon rolling of the sheets into tubes is stabilized by enhanced chromophore interactions.

This comparison gives a good explanation not only on how the introduction of hydrogen bonding OH groups can direct the formation of planar sheets in case of a chiral compound but also on why the formation of tubular aggregates is preferred by the achiral mesomer. In this respect as well as regarding the aggregation behaviour of the parent C8O3/S3 dyes, which both form only tubular aggregates, one can suspect that the formation of tubes may be an intrinsic property of the hydrophobic dye skeletons with their hydrocarbon chains rather than being provoked by the hydrophilic head groups. The observation that the diameter of monolayered tubes (of the bundles) and of the inner cylinders of the bilayered tubes are identical points at comparable chromophore interactions in both architectures. The initial twist in the monolayered inverted tube bundles, however, gives direct structural evidence for a chiral packing principle in both tubular assembly structures. It is, however, still not clear what drives the assembly process of the mesomer into two structurally different species (individual tubes and bundles).

#### V. Conclusion

We have synthesized a new group of TBC based amphiphilic cyanine dye derivatives by converting the anionic carboxylic acid groups into non-ionic hydroxyl functionalities. The compounds contain amino-propanediol groups which provide sufficient water solubility and defined chirality. To produce the achiral meso-form of the dye a new synthetic route towards asymmetrically functionalized TBC dyes was established.

All compounds form J-aggregates in water. Cryo-TEM revealed the formation of extended sheet-like aggregates for the chiral enantiomers (**1a** and **1b**) and individual tubes with 12 - 13 nm diameter as well as tube bundles for the mesomer (**1c**). In case of the conformer (**2**) needle-like crystals predominate by far.

Our findings demonstrate that the supramolecular aggregation behaviour of cyanine dyes can be controlled solely by stereochemistry. The surprising aspect is the inverse relationship between molecular chirality and helicity of the supramolecular architecture. The reason is obviously the special interaction of the non-ionic hydroxyl functionalities. In case of the chiral enantiomers (**1a** and **1b**) extended hydrogen bond chains can interconnect molecules in a brickwork arrangement. This yields a two-dimensional planar network which prevents the spontaneous formation of curved assemblies like the tubes and tubes bundles formed by the meso-form (**1c**) which is not capable of forming comparable hydrogen bond chains.

Absorption, LD and fluorescence spectra of the tubes point to a monolayered architecture, although single tubes clearly show a double-layer wall geometry. In recent literature<sup>[5e]</sup> this apparent contradiction has been resolved by the evidence of a dominating population of tube bundles. Supported by cryo-ET it was observed that during the hierarchical assembly of the



bilayered C8S3 tubes into bundles the outer monolayer is lost. The present cryo-ET investigation and the structural analysis of similar bundled aggregates not only affirms this interpretation but adds evidence for a tight packing of the hydrophobic cylinders.

The new insights into the interdependence of stereochemistry and supramolecular aggregation behaviour of cyanine dyes might contribute to the development of specialised, dye-based materials with predictable properties.

## VI. Experimental Section

### *Materials and methods*

**Materials.** Dry solvents and chemicals were purchased from Sigma-Aldrich, TCI and abcr Chemicals. Ethyl acetate, hexane, and dichloro methane were distilled before utilisation in reactions as well as in compound purifications. Enantiopure R- and S-solketal were purchased from TCI with 98 % *ee* optical purity. C8O3 was obtained from FEW chemicals (Wolfen, Germany). Reactions were monitored using thin layer chromatography on silica coated aluminium sheets using 60 F254 silica gel or 60 RP-18 F254S silica gel for reverse phase analysis. All intermediates were purified using normal phase column chromatography and automated flash chromatography on a combi Flash Rf column (Teledyne ISCO) packed with normal silica gel (30  $\mu\text{m}$ ). The final products were purified using reverse phase preparative HPLC.

**NMR-spectroscopy.**  $^1\text{H}$  NMR and  $^{13}\text{C}$  NMR were recorded on a JEOL ECP 500 spectrometer (500 MHz); mass spectra were recorded using an Agilent 6210 ESI-TOF spectrometer.

**Sample preparation.** Dye stock solutions were prepared from dried solid matter and the respective solvent by vigorously shaking the samples. For spectroscopic measurements, the solutions were diluted, if necessary.

**Spectroscopic measurements.** Isotropic absorption spectra (UV/vis) were measured on a Varian Cary<sup>®</sup> 50 spectrophotometer (Agilent Technologies Inc., Santa Clara, USA), fluorescence spectra on a luminescence spectrometer LS 50B (Perkin Elmer, Rodgau, Germany). Circular dichroism (CD) and linear dichroism (LD) were measured on a J-810 spectropolarimeter (Jasco Corp., Tokyo, Japan), which could be equipped with a microvolume Couette flow LD cell (Dioptica Scientific Limited, Rugby, Warwickshire, UK) with 0.5 mm optical path length for the LD measurement.<sup>[26]</sup> The LD spectra were independent of the angular velocity of the rotating cell. Rotating velocities up to 3000 rpm, corresponding to shear forces of  $\sim 1200\text{ s}^{-1}$ , were used. CD measurements were carried out at 20°C, all other spectroscopic measurements at room temperature ( $22 \pm 1^\circ\text{C}$ ). Cuvettes for UV/vis, fluorescence, and CD were siliconized before measurements according to the "Siliconization of Glasware"-protocol using a silicone solution in isopropanol (SERVA Electrophoresis GmbH, Heidelberg, Germany).

**Cryo-Transmission Electron Microscopy (cryo-TEM).** 200 mesh grids covered with perforated carbon film (R1/4 batch of Quantifoil, MicroTools GmbH, Jena, Germany) were cleaned with chloroform and hydrophilized by 60 s glow discharging at 8 W in a BAL-TEC MED 020 device (Leica Microsystems, Wetzlar, Germany). After applying 5  $\mu\text{l}$  aliquots of the dye solution to the grids the samples were vitrified by automated blotting and plunge freezing in to liquid ethane by use of a FEI Vitrobot Mark IV (Thermo Fisher Scientific Inc., Waltham, Massachusetts, USA). The vitrified specimens were transferred under liquid nitrogen to a FEI TALOS L120C electron microscope (Thermo Fisher Scientific Inc., Waltham, Massachusetts, USA) using a Gatan cryo-holder and stage (model 626, Gatan, Inc., Pleasanton, California, USA). The microscope was equipped with a LaB6 cathode and operated at 120 kV accelerating voltage. Micrographs were acquired on a FEI Ceta CMOS camera (Thermo Fisher Scientific Inc., Waltham, Massachusetts, USA) at a nominal magnification of 36,000  $\times$ , corresponding to a calibrated pixel size of 4.09  $\text{\AA}/\text{pixel}$ .

**Cryo-Electron Tomography (cryo-ET).** Vitrified specimen (see above) intended for cryo-ET were transferred to the autoloader of a FEI TALOS ARCTICA electron microscope (Thermo Fisher Scientific Inc., Waltham, Massachusetts, USA). This microscope is equipped with a high-brightness field-emission gun (XFEG) operated at an acceleration voltage of 200 kV. Micrographs were acquired on a FEI Falcon 3 direct electron detector (Thermo Fisher Scientific Inc., Waltham, Massachusetts, USA) at a nominal magnification of 28,000  $\times$ , corresponding to a calibrated pixel size of 3.64  $\text{\AA}/\text{pixel}$ .

Tomography series were recorded in the context of FEI Tomography Software V 4.3.1. 4096  $\times$  4096 pixel images were recorded in the tilt angle range of  $\pm 65^\circ$  in  $2^\circ$  increments with a total electron dose of 180  $\text{e}/\text{\AA}^2$ . 3D volume reconstructions were calculated with the help of INSPECT3D Software V4.4 (Thermo Fisher Scientific Inc., Waltham, Massachusetts, USA) and visualized with Imod V4.9.10<sup>[27]</sup>.

**Image processing.** Each three consecutive slices of the tomogram along the tube bundle were summed and cropped using the slicer of Imod V4.9.10.<sup>[27]</sup> The cross-sectional motif of the bundle was boxed off these images using the boxer module of the EMAN software package.<sup>[28]</sup> Alignments, multivariate statistical analysis (MSA) of a total of 232 such motifs, summing, and finally construction of a twisted 3D volume of the bundle with a pitch of 400 nm was performed with the Imagic 5 Software package (Image Science Software GmbH, Berlin, Germany). The resulting 3D volume was visualized using AMIRA Software V2019.1 (Thermo Fisher Scientific Inc., Waltham, Massachusetts, USA).

**Atomic Force Microscopy (AFM).** Atomic force microscopy was carried out with a Multimode 8 Nanoscope with Nanocontroller V (Bruker, Billerica, Massachusetts, USA) and equipped with ultra-sharp PEAKFORCE-HIRS-F-B tips (Bruker) providing a nominal radius of 1 nm and maximum radius of 2 nm. The sample was prepared by deposition of 10  $\mu\text{l}$  of the 0.1 mM aqueous dye solution on cleaved mica which was glued on a circular metal disk with double

sided tape. The dye assemblies were allowed to settle for about 5 minutes before the solution was blotted with filter paper until only a thin solution film was left. The sample was then immediately mounted on the AFM scanner and a liquid chamber was assembled and carefully filled with Milli-Q water to prevent drying of the sample. Imaging was performed with a calibrated cantilever<sup>[29]</sup> in *PeakForce* Quantitative NanoMechanics (QNM) mode,<sup>[30]</sup> in order to control the loading force on the sample at all times. The maximum loading force used was 500 pN, the resolution was 512 points per line, and the scan rate was 0.7 Hz.

### Synthesis

**Compounds 3a and 3b.** Enantiopure Solketal (R or S) was converted into the corresponding phthalimide according to the published procedure from Goubert *et al.*<sup>[31]</sup>

**Compound 3a.** Using (R)-(-)-2,2-dimethyl-1,3-dioxolane-4-methanol (4.2 g, 31.8 mmol) the corresponding phthalimide **3a** was obtained as a colorless solid (7.6 g, 92 %). <sup>1</sup>H NMR (500 MHz, Chloroform-d)  $\delta$  7.84 (dd, J = 5.4, 3.0 Hz, 2H), 7.71 (dd, J = 5.5, 3.0 Hz, 2H), 4.49-4.38 (m, 1H), 4.06 (dd, J = 8.7, 6.2 Hz, 1H), 3.92 (dd, J = 13.8, 6.9 Hz, 1H), 3.84 (dd, J = 8.7, 5.1 Hz, 1H), 3.71 (dd, J = 13.8, 5.3 Hz, 1H), 1.43 (s, 3H), 1.30 (s, 3H); <sup>13</sup>C NMR (126 MHz, Chloroform-d)  $\delta$  168.33, 134.16, 132.12, 123.49, 109.95, 73.43, 67.49, 41.09, 26.95, 25.49. MS m/z 284.0898 (calcd. C<sub>14</sub>H<sub>15</sub>NNaO<sub>4</sub><sup>+</sup> 284.0893).

**Compound 3b.** Using (S)-(+)-2,2-dimethyl-1,3-dioxolane-4-methanol (2.0 g, 15.1 mmol) the corresponding phthalimide **3b** was obtained as a colorless solid (3.3 g, 83 %). <sup>1</sup>H NMR (500 MHz, Chloroform-d)  $\delta$  7.84 (dd, J = 5.5, 3.0 Hz, 2H), 7.71 (dd, J = 5.5, 3.0 Hz, 2H), 4.49-4.38 (m, 1H), 4.06 (dd, J = 8.7, 6.2 Hz, 1H), 3.92 (dd, J = 13.8, 6.9 Hz, 1H), 3.84 (dd, J = 8.7, 5.1 Hz, 1H), 3.71 (dd, J = 13.8, 5.3 Hz, 1H), 1.43 (s, 3H), 1.30 (s, 3H); <sup>13</sup>C NMR (126 MHz, Chloroform-d)  $\delta$  168.33, 134.16, 132.12, 123.49, 109.95, 73.43, 67.49, 41.09, 26.95, 25.49. MS m/z 284.0891 (calcd. C<sub>14</sub>H<sub>15</sub>NNaO<sub>4</sub><sup>+</sup> 284.0893).

**Compounds 4a and 4b.** 2-((2,2-dimethyl-1,3-dioxolan-4-yl)methyl)isoindoline-1,3-dione **3** (**a** or **b**) were reacted according to the procedure published in literature.<sup>[31]</sup>

**Compound 4a.** Using S-phthalimide **3a** (1.4 g, 5.4 mmol) the corresponding amine **4a** was obtained as a pale-yellow liquid (0.3 g, 43 %). <sup>1</sup>H NMR (500 MHz, Methanol-d<sub>4</sub>)  $\delta$  4.14 (qd, J = 6.4, 4.8 Hz, 1H), 4.05 (dd, J = 8.3, 6.4 Hz, 1H), 3.65 (dd, J = 8.3, 6.3 Hz, 1H), 2.81 – 2.64 (m, 2H), 1.39 (s, 3H), 1.33 (s, 3H); <sup>13</sup>C NMR (126 MHz, Methanol-d<sub>4</sub>)  $\delta$  110.33, 78.06, 68.04, 45.21, 27.18, 25.57. MS m/z 132.1008 (calcd. C<sub>6</sub>H<sub>14</sub>NO<sub>2</sub><sup>+</sup> 132.1019).

**Compound 4b.** Using R-phthalimide **3b** (1.0 g, 3.9 mmol) the corresponding amine **4b** was obtained as a pale-yellow liquid (0.28 g, 55 %).  $^1\text{H}$  NMR (500 MHz, Methanol- $d_4$ )  $\delta$  4.13 (qd,  $J$  = 6.4, 4.8 Hz, 1H), 4.04 (dd,  $J$  = 8.2, 6.4 Hz, 1H), 3.65 (dd,  $J$  = 8.2, 6.4 Hz, 1H), 2.80 – 2.64 (m, 2H), 1.39 (s, 3H), 1.33 (s, 3H);  $^{13}\text{C}$  NMR (126 MHz, Methanol- $d_4$ )  $\delta$  110.30, 78.16, 68.05, 45.25, 27.17, 25.57. MS  $m/z$  132.1037 (calcd.  $\text{C}_6\text{H}_{14}\text{NO}_2^+$  132.1019).

**Compounds 5a and 5b.** To a solution of 30 mg (0.037 mmol) C8O3, 48 mg (0.126 mmol) HATU and 48.5 mg (0.370 mmol) solketal-amine **4 (a or b)** in 3 mL DMF was added (0.518 mmol) DIPEA and the mixture was stirred at r.t. for 2 h. After removal of the solvent in vacuum, the residue was dissolved in  $\text{CH}_2\text{Cl}_2$  and washed with water three times. The combined organic phases were concentrated, and the residue was purified by automated column chromatography ( $\text{CH}_2\text{Cl}_2$ /methanol, 0-5 %).

**Compound 5a.** Solketal amine **4a** was reacted according to the above-described procedure and dye **5a** was obtained as a red solid (36 mg, 91 %).  $^1\text{H}$  NMR (700 MHz, Methanol- $d_4$ )  $\delta$  8.00 (s, 1H), 7.76 (s, 2H), 7.73 (s, 2H), 4.31 (dt,  $J$  = 14.9, 7.5 Hz, 8H), 4.10 (p,  $J$  = 5.8 Hz, 2H), 3.97 (dd,  $J$  = 8.4, 6.3 Hz, 2H), 3.60 (dd,  $J$  = 8.4, 5.9 Hz, 2H), 3.28-3.20 (m, 4H), 2.39 (t,  $J$  = 6.7 Hz, 4H), 2.14 (p,  $J$  = 6.9 Hz, 4H), 1.87 (p,  $J$  = 7.4 Hz, 4H), 1.45 – 1.21 (m, 32H), 0.86 (t,  $J$  = 7.0 Hz, 6H);  $^{13}\text{C}$  NMR (176 MHz, Methanol- $d_4$ )  $\delta$  174.41, 151.36, 144.06, 133.78, 133.60, 128.69, 116.58, 112.56, 110.48, 75.88, 68.15, 46.31, 45.74, 43.00, 32.93, 32.73, 30.76, 30.35, 29.09, 27.66, 27.20, 25.56, 24.62, 23.68, 14.42. MS  $m/z$  1035.4713 (calcd.  $\text{C}_{53}\text{H}_{77}\text{Cl}_4\text{N}_6\text{O}_6^+$  1035.4624).

**Compound 5b.** Solketal amine **4b** (48.5 mg, 0.370 mmol) was reacted according to the above-described procedure and dye **5b** was obtained as a red solid (32 mg, 81 %).  $^1\text{H}$  NMR (700 MHz, Methanol- $d_4$ )  $\delta$  8.01 (s, 1H), 7.76 (s, 2H), 7.73 (s, 2H), 5.82 (d,  $J$  = 13.3 Hz, 2H), 4.31 (dt,  $J$  = 14.0, 8.0 Hz, 8H), 4.10 (p,  $J$  = 5.8 Hz, 2H), 3.97 (dd,  $J$  = 8.4, 6.3 Hz, 2H), 3.60 (dd,  $J$  = 8.4, 5.9 Hz, 2H), 3.26 – 3.21 (m, 4H), 2.38 (t,  $J$  = 6.8 Hz, 4H), 2.14 (p,  $J$  = 7.0 Hz, 4H), 1.87 (p,  $J$  = 7.3 Hz, 4H), 1.45 – 1.21 (m, 32H), 0.85 (t,  $J$  = 6.9 Hz, 6H);  $^{13}\text{C}$  NMR (176 MHz, Methanol- $d_4$ )  $\delta$  174.46, 151.29, 133.79, 133.56, 128.90, 128.64, 112.51, 110.47, 75.85, 68.16, 46.31, 45.66, 42.99, 32.91, 32.71, 30.39, 30.27, 29.07, 27.62, 27.19, 25.57, 24.62, 23.67, 14.42. MS  $m/z$  1035.4797 (calcd.  $\text{C}_{53}\text{H}_{77}\text{Cl}_4\text{N}_6\text{O}_6^+$  1035.4624).

**Compounds 1a and 1b.** Hydrogen chloride (1.301 mmol) was added to a solution of dye **5 (a or b)** (0.033 mmol) in 100 mL methanol and the mixture was stirred at r.t. for 3 h. The solvents

were removed in vacuum by distillation with toluene and the crude product was lyophilized. The obtained residue was purified by reversed-phase column chromatography using water/acetonitrile (75%) and 50mM ammonium formate.

**Compound 1a.** Dye **5a** (35 mg, 0.033 mmol) was reacted according to the procedure described above. Dye **1a** was obtained as a red solid (31.4 mg, 96 %).  $^1\text{H}$  NMR (700 MHz, Methanol- $d_4$ )  $\delta$  8.46 (m, 1H), 8.40-8.38 (m, 2H), 8.36 (m, 1H), 7.25 (s, 1H), 4.71-4.53 (m, 8H), 3.65-3.58 (m, 3H), 3.49-3.43 (m, 3H), 3.20 (m, 2H), 3.01-2.99 (m, 1H) 2.88-2.86 (m, 1H), 2.52-2.41 (m, 4H), 2.29-2.15 (m, 4H), 2.04-1.91 (m, 4H), 1.42-1.30 (m, 20H), 0.92-0.88 (m, 6H).  $^{13}\text{C}$  NMR (176 MHz, MeOD)  $\delta$  = 173.24, 150.54, 148.03, 141.40, 136.49, 131.82, 131.55, 131.35, 131.20, 131.08, 130.67, 115.35, 115.05, 70.51, 63.62, 55.76, 42.01, 31.53, 29.15, 28.78, 26.25, 22.43, 13.13. MS  $m/z$  955.4044 (calcd.  $\text{C}_{47}\text{H}_{69}\text{Cl}_4\text{N}_6\text{O}_6^+$  955.3998).

**Compound 1b.** Dye **5b** (30 mg, 0.028 mmol) was reacted according to the procedure described above. Dye **1b** was obtained as a red solid (26.1 mg, 94 %).  $^1\text{H}$  NMR (700 MHz, Methanol- $d_4$ )  $\delta$  8.44 (s, 1H), 8.38 (s, 1H), 8.37 (s, 1H), 8.33 (s, 1H), 7.23 (s, 1H), 4.68-4.49 (m, 8H), 3.62-3.56 (m, 2H), 3.44-3.42 (m, 4H), 3.26-3.25 (m, 1H) 3.17-3.14 (m, 1H), 3.00-2.97 (m, 1H), 2.86-2.83 (m, 1H), 2.52-2.42 (m, 4H), 2.25-2.13 (m, 4H), 1.99-1.90 (m, 4H), 1.52-1.29 (m, 20, H), 0.90-0.88 (m, 6H).  $^{13}\text{C}$  NMR (176 MHz, Methanol- $d_4$ )  $\delta$  174.61, 174.05, 151.87, 149.39, 142.97, 132.92, 132.89, 132.78, 132.72, 132.44, 132.38, 132.36, 132.33, 116.44, 116.29, 116.23, 71.93, 71.83, 65.02, 47.92, 47.34, 46.95, 43.37, 43.07, 32.95, 32.39, 32.14, 30.46, 30.41, 30.37, 30.34, 27.69, 25.90, 25.40, 23.70, 14.41. MS  $m/z$  955.4044 (calcd.  $\text{C}_{47}\text{H}_{69}\text{Cl}_4\text{N}_6\text{O}_6^+$  955.3998).

**Compound 2.** To a solution of 30 mg (0.037 mmol)  $\text{C}_8\text{O}_3$ , 48 mg (0.126 mmol) HATU, and 34 mg (0.370 mmol) serinol in 3 mL DMF 88.2  $\mu\text{L}$  (0.518 mmol) DIPEA was added and the mixture was stirred at r.t. for 2 h. After removal of the solvent in vacuum, the residue was purified by reversed-phase column chromatography using water/acetonitrile (75%) and 50mM ammonium formate to give compound **2** as red solid (16 mg, 44 %).  $^1\text{H}$  NMR (700 MHz, Methanol- $d_4$ )  $\delta$  8.50 (s, 1H), 7.99 (s, 1H), 7.78 (s, 2H), 7.74 (s, 2H), 4.35 – 4.28 (m, 12H), 3.92 (p,  $J$  = 5.6 Hz, 2H), 3.60 (dd,  $J$  = 11.0, 5.4 Hz, 4H), 3.57 (dd,  $J$  = 11.1, 5.8 Hz, 4H), 2.42 (t,  $J$  = 6.9 Hz, 4H), 2.14 (p,  $J$  = 7.2 Hz, 4H), 1.87 (p,  $J$  = 6.9 Hz, 4H), 1.44 – 1.21 (m, 20H), 0.86 (t,  $J$  = 6.9 Hz, 6H);  $^{13}\text{C}$  NMR (176 MHz, Methanol- $d_4$ )  $\delta$  174.43, 170.27, 151.33, 151.27, 133.81, 133.55, 128.73, 112.57, 62.09, 54.50, 46.33, 45.67, 33.00, 32.92, 30.38, 30.29, 29.06, 27.65, 24.78, 23.67, 14.41. MS  $m/z$  955.4007 (calcd.  $\text{C}_{47}\text{H}_{69}\text{Cl}_4\text{N}_6\text{O}_6^+$  955.3998).

**Compound 6.** To a stirred solution of 5,6-dichlorobenzimidazole (5 g, 24.8 mmol, 1 eq) in DMSO the required amount of NaOH (1.09 g, 27.3 mmol, 1.1 eq) was added. The reaction solution was stirred for 2 h at room temperature. Thereafter, the calculated amount of ethyl 4-bromobutanoate (5.82 g, 28.5 mmol, 1.2 eq) was added and the reaction mixture was left stirring for 48 h at room temperature. Progress of the reaction was monitored by TLC using methanol/dichloromethane. On completion of the reaction, the mixture was suspended in water and ethyl acetate (3x30 mL). The combined organic layers were dried over anhydrous sodium sulphate and the solvent was evaporated to yield the crude product, which was purified through column chromatography using DCM and methanol to give compound **6** as a white solid in 95% yield.  $^1\text{H}$  NMR (500 MHz, methanol- $d_3$ )  $\delta$  7.66 (s, 1H), 7.61 (s, 1H), 4.20 (t,  $J = 7.45$ , 3H), 4.07-4.02 (q, 2H), 2.59 (s, 3H), 2.41 (t,  $J = 6.70$ , 2H), 2.08-2.02 (m, 2H), 1.20 (t,  $J = 7.15$ , 3H);  $^{13}\text{C}$  NMR (126 MHz, methanol- $d_3$ )  $\delta$  174.23, 156.04, 142.27, 135.63, 127.11, 126.82, 120.08, 112.66, 61.72, 44.16, 31.48, 25.41, 14.43, 13.52. MS  $m/z$  315.0589 (calcd.  $\text{C}_{14}\text{H}_{17}\text{Cl}_2\text{N}_2\text{O}_2^+$  315.0361).

**Compound 7.** Compound **6** (2 g, 6.34 mmol, 1 eq) was liquefied at 150 °C. 1-Bromodecane (7.0 g, 31.7 mmol, 5 eq) was added to the reaction flask and the reaction mixture was left stirring at 150 °C for 6 h. After completion of the reaction (indicated by TLC using methanol/dichloromethane) the reaction mixture was extracted with water and dichloromethane (3 × 50 mL). The combined organic layers were dried over anhydrous sodium sulphate and the solvent evaporated to yield the crude product, which was further purified through column chromatography using DCM and methanol as eluent to give compound **7** as a light yellowish solid in 72% yield.  $^1\text{H}$  NMR (500 MHz, Chloroform- $d_3$ )  $\delta$  8.22 (s, 1H), 7.81 (s, 1H), 4.66 (t,  $J = 7.75$ , 3H), 4.44 (t,  $J = 7.45$ , 3H), 3.99-3.95 (q, 2H), 2.55 (t,  $J = 6.50$ , 2H), 2.13-2.07 (m, 2H), 1.82-1.76 (m, 2H), 1.36-1.30 (m, 2H), 1.25-1.11 (m, 13H), 0.77 (t,  $J = 4.55$ , 3H);  $^{13}\text{C}$  NMR (126 MHz, Chloroform- $d_3$ )  $\delta$  172.68, 153.09, 131.36, 131.30, 130.30, 130.14, 114.91, 114.04, 77.41, 77.16, 76.90, 60.71, 47.08, 45.87, 31.57, 30.22, 28.99, 28.90, 26.61, 23.91, 22.44, 14.03, 13.93, 12.96. MS  $m/z$  428.1876 (calcd.  $\text{C}_{22}\text{H}_{34}\text{Cl}_2\text{N}_2\text{O}_2^+$  428.1914)

**Compound 8.** Compound **7** (1 g 1.8 mmol, 1 eq) was stirred with a 1:1 mixture of HBr (48%) and water at 120 °C for 15 h. Progress of the reaction was monitored by TLC using methanol/dichloromethane. On completion of the reaction, the reaction mixture was cooled to room temperature. The precipitate was filtered and washed with aq. hydrobromic acid (5%

w/w) to yield compound **8** as light yellowish solid in 98% yield.  $^1\text{H}$  NMR (500 MHz, methanol- $d_3$ )  $\delta$  8.35 (s, 1H), 8.30 (s, 1H), 4.55 (t,  $J = 7.77$  Hz, 2H), 4.48 (t,  $J = 7.65$  Hz, 2H), 2.98 (s, 3H), 2.54 (t,  $J = 6.45$  Hz, 2H), 2.19-2.13 (m, 2H), 1.93-1.86 (m, 2H), 1.48-1.32 (m, 12H), 0.91 (t,  $J = 6.85$  Hz, 3H);  $^{13}\text{C}$  NMR (126 MHz, methanol- $d_3$ )  $\delta$  174.69, 153.17, 130.70, 114.64, 45.96, 45.02, 31.58, 29.57, 28.94, 28.73, 26.24, 23.54, 22.39, 13.03, 9.76. MS  $m/z$  400.1601 (calcd.  $\text{C}_{20}\text{H}_{30}\text{Cl}_2\text{N}_2\text{O}_2^+$  400.1608).

**Compound 9.** To a stirred solution of compound **6** (2.5 g, 7.9 mmol, 1 eq) in ethanol, the required amount of KOH (0.88 g, 15.8 mmol, 2 eq) was added. The reaction solution was stirred for 12 h at refluxing temperature. Progress of the reaction was indicated by TLC using methanol/dichloromethane. On completion, the reaction mixture was neutralized using Dowex-50 cation exchange resin. The resin was filtered, and the filtrate was concentrated under reduced pressure to give compound **9** as an off-white solid in 95% yield.  $^1\text{H}$  NMR (500 MHz, methanol- $d_3$ )  $\delta$  7.76 (s, 1H), 7.66 (s, 1H), 4.24 (t,  $J = 7.55$  Hz, 2H), 2.60 (s, 3H), 2.08, 2.06-2.02 (m, 2H);  $^{13}\text{C}$  NMR (126 MHz, methanol- $d_3$ )  $\delta$  174.79, 154.79, 140.91, 134.38, 125.80, 118.76, 111.51, 42.88, 29.85, 24.29, 12.11. MS  $m/z$  287.0276 (calcd.  $\text{C}_{12}\text{H}_{13}\text{Cl}_2\text{N}_2\text{O}_2$  287.0266).

**Compound 10.** To a stirred solution of compound **9** (2.0 g, 6.94 mmol, 1 eq) in DMF (30 mL), (S) solketal amine, EDC.HCl (2.0 g, 10.4 mmol, 1.5 eq), and DMAP (0.45 g, 3.4 mmol, 0.5 eq) were added at room temperature. The reaction mixture was left stirring for 24 h. Progress of the reaction was monitored by TLC using methanol/dichloromethane. On completion, the mixture was suspended in water and DCM ( $3 \times 30$  mL). The combined organic layers were dried over anhydrous sodium sulphate and the solvent evaporated to yield the crude product, which was purified through column chromatography using DCM and methanol to give compound **10** as a white solid in 75% yield.  $^1\text{H}$  NMR (500 MHz, chloroform- $d_3$ )  $\delta$  7.64, 7.37, 7.26, 6.11 (t,  $J = 5.6$  Hz, 1H), 4.19-4.14 (m, 1H), 4.10 (t,  $J = 7.2$  Hz, 2H), 4.02-3.99 (m, 1H), 3.59-3.56 (m, 1H), 3.55-3.51 (m, 1H), 3.22-3.17 (m, 1H), 2.52 (s, 3H), 2.18 (t,  $J = 6.8$ , 3H), 2.08-2.03 (m, 2H), 1.35 (s, 3H), 1.28 (s, 3H);  $^{13}\text{C}$  NMR (126 MHz, chloroform- $d_3$ )  $\delta$  171.44, 153.82, 141.95, 134.49, 126.02, 125.83, 120.11, 110.73, 109.53, 77.44, 77.18, 76.93, 74.54, 66.80, 43.22, 42.04, 32.00, 26.88, 25.14, 24.89, 13.90. MS  $m/z$  400.1116 (calcd.  $\text{C}_{18}\text{H}_{24}\text{Cl}_2\text{N}_3\text{O}_3^+$  400.1218)

**Compound 11.** Compound **10** (1.5 g, 6.34 mmol, 1 eq) was liquefied at 150 °C. 1-Bromodecane (7.0 g, 31.7 mmol, 5 eq) was added to the reaction flask and the reaction mixture was left

stirring at 150 °C for 6 h. Progress of the reaction was monitored by TLC using methanol/dichloromethane. Upon completion of the reaction, the mixture was extracted with water and dichloromethane (3x50 mL). The combined organic layers were dried over anhydrous sodium sulphate and the solvent evaporated to yield the crude product, which was further purified through column chromatography using DCM and methanol as eluent to give compound **11** as a white solid in 65% yield.  $^1\text{H}$  NMR (500 MHz, chloroform- $d_3$ )  $\delta$  8.18 (s, 1H), 7.77 (s, 1H), 7.50 (t,  $J = 5.9$  Hz, 1H), 4.62 (t,  $J = 7.1$  Hz, 2H), 4.42 (t,  $J = 7.5$  Hz, 2H), 4.16-4.12 (m, 1H), 3.98-3.95 (m, 1H), 3.66-3.64 (m, 1H), 3.26 (t,  $J = 5.9$  Hz, 2H), 2.53 (t,  $J = 6.9$  Hz, 2H), 2.23-2.18 (m, 2H), 1.87-1.81 (m, 2H), 1.37-1.22 (m, 18H), 0.83 (t,  $J = 6.9$  Hz, 3H);  $^{13}\text{C}$  NMR (126 MHz, chloroform- $d_3$ )  $\delta$  172.15, 153.00, 131.78, 130.38, 130.30, 115.06, 114.02, 109.29, 77.41, 77.16, 76.91, 74.42, 67.60, 47.23, 46.25, 42.03, 32.07, 31.70, 29.09, 29.05, 27.00, 26.81, 25.42, 24.81, 22.58, 14.07, 12.90. MS  $m/z$  512.2441 (calcd.  $\text{C}_{26}\text{H}_{40}\text{Cl}_2\text{N}_2\text{O}_3^+$  512.2455).

**Compound 12.** Compound **8** (0.5 g, 0.001 mmol, 1eq) and compound **11** (0.5 g, 0.008 mmol, 1eq) were weighed in round bottom flask.  $\text{CH}_3\text{I}$  (0.18 g, 0.0004 mmol, 0.45 eq) and DBU (1.1 g, 0.007, 7 eq) were added to the reaction flask followed by addition of methanol (25mL) as a solvent. The reaction mixture was left stirring at room temperature for 48 h. Progress of the reaction was monitored by TLC using methanol/dichloromethane. Upon completion of the reaction, the mixture was the crude product, which was purified through column chromatography using DCM and methanol to give compound **12** as a white solid in 11% yield.  $^1\text{H}$  NMR (500 MHz, methanol- $d_4$ )  $\delta$  8.34 (s, 2H), 8.29 (s, 2H), 4.55-4.47 (m, 8H), 4.12-4.07 (m, 1H), 4.01-3.98 (m, 1H), 3.62-3.60 (m, 1H), 3.24-3.22 (d, 2H), 2.45 (t,  $J = 6.7$  Hz, 4H), 2.21-2.16 (m, 4H), 1.93-1.87 (m, 4H), 1.50-1.45 (m, 4H), 1.43-1.30 (m, 20H), 0.90 (t,  $J = 6.8$  Hz, 6H);  $^{13}\text{C}$  NMR (126 MHz, methanol- $d_3$ )  $\delta$  173.01, 130.79, 130.76, 130.72, 114.66, 114.61, 109.20, 74.50, 66.88, 48.22, 48.05, 47.95, 47.94, 47.93, 47.93, 47.92, 47.91, 47.88, 47.85, 47.84, 47.83, 47.71, 47.54, 47.37, 47.20, 46.16, 45.43, 41.67, 31.60, 31.48, 28.97, 28.91, 28.80, 26.29, 25.91, 24.30, 24.01, 22.35, 13.11. MS  $m/z$  922.3812 (calcd.  $\text{C}_{53}\text{H}_{77}\text{Cl}_4\text{N}_6\text{O}_6^+$  922.3783).

**Compound 13.** To a stirred solution of compound **12** (0.060 g, 0.005 mmol, 1 eq) in DMF (30 mL), (R) solketal amine (0.114 g, 0.086 mmol, 1.5 eq), EDC.HCl (0.172 g, 0.086 mmol, 1.5 eq) and DMAP (0.035g, 0.028 mmol, 0.5 eq) were added at room temperature. The reaction mixture was left stirring for 24 h. Progress of the reaction was monitored by TLC using methanol/dichloromethane. Upon completion of the reaction, the mixture was suspended in



water and DCM (3×30 mL). The combined organic layers were dried over anhydrous sodium sulphate and the solvent evaporated to yield the crude product, which was purified through column chromatography using DCM and methanol to give compound **13** as a red solid in 77% yield. <sup>1</sup>H NMR (500 MHz, methanol-d<sub>4</sub>) δ 8.01 (s, 1H), 7.78 (s, 2H), 7.75 (s, 2H), 4.36-4.30 (m, 8H), 4.13-4.11 (m, 2H), 4.00-3.97 (dd, J = 8.4, 6.3 Hz, 2H), 3.64-3.61 (dd, J = J = 8.4, 6.0 Hz, 2H), 3.27-3.25 (m, 2H), 2.41 (t, J = 6.7 Hz, 4H), 2.19-2.13 (p, J = 6.7 Hz, 4H), 1.92-1.86 (p, J = 6.4, 4H), 1.42-1.27 (m, 32H), 0.87 (t, J = 6.8 Hz, 6H); <sup>13</sup>C NMR (126 MHz, chloroform-d<sub>3</sub>) δ = 174.47, 133.77, 133.53, 128.63, 112.52, 110.47, 75.84, 68.17, 49.51, 49.17, 49.00, 48.83, 48.49, 46.36, 45.71, 42.98, 32.90, 32.78, 30.38, 30.26, 29.07, 27.64, 27.21, 25.59, 24.67, 23.65, 14.44. MS m/z 1035.4696 (calcd. C<sub>53</sub>H<sub>77</sub>Cl<sub>4</sub>N<sub>6</sub>O<sub>6</sub><sup>+</sup> 1035.4624).

**Compound 1c.** Hydrogen chloride (1.301 mmol) was added to a solution of dye (**13**) (0.033 mmol) in 100 mL methanol and the mixture was stirred at r.t. for 3 h. The solvents were removed in vacuum by distillation with toluene and the crude product was lyophilized and further purified with reverse phase HPLC using 95 % MeCN and water as eluent and ammonium formate as a modifier. The desired compound **1c** was obtained as a red solid in 37% yield. <sup>1</sup>H NMR (600 MHz, methanol-d<sub>4</sub>) δ 8.50 (s, 1H), 7.96 (s, 1H), 7.74 (s, 2H), 7.71 (s, 2H), 4.30-4.27 (m, 8H), 3.99-3.98 (m, 1H), 3.65-3.61 (m, 3H), 3.43-3.42 (m, 4H), 3.15-3.12 (m, 2H), 2.38 (m, 4H), 2.14 2.09 (m 4H), 1.87-1.82, (m, 4H), 1.36-1.24 (m, 20H), 0.83 (t, J = 6.8 Hz, 6H); <sup>13</sup>C NMR (176 MHz, MeOD) δ = 173.33, 149.87, 147.90, 136.43, 132.83, 132.45, 132.29, 131.48, 131.07, 130.94, 127.37, 122.32, 115.19, 111.17, 70.52, 63.62, 45.00, 44.10, 42.04, 31.50, 29.33, 29.13, 28.97, 28.86, 28.74, 27.64, 26.36, 26.09, 25.07, 24.66, 23.38, 22.26, 13.02. MS m/z 955.3981 (calcd. C<sub>47</sub>H<sub>69</sub>Cl<sub>4</sub>N<sub>6</sub>O<sub>6</sub><sup>+</sup> 955.3998).

## VII. Acknowledgement

This work was supported by the Deutsche Forschungsgemeinschaft (DFG) by means of financial support to the projects of C. B. (BO 1000/11-1) and R. H. (HA 2549/18-1).

## VIII. References

- [1] a) E. E. Jelly, *Nature* **1936**, *138*, 1009-1010; b) G. Scheibe, *Angew. Chem.* **1936**, *49*, 563; c) F. Würthner, T. E. Kaiser, C. R. Saha-Möllner, *Angew. Chem. Int. Ed. Engl.* **2011**, *50*, 3376-3410.
- [2] E. G. McRae, M. Kasha, *J. Chem. Phys.* **1958**, *28*, 721-722.
- [3] J. L. Bricks, Y. L. Slominsky, I. Panas, A. Demchenko, *Methods and Applications in Fluorescence* **2017**.
- [4] A. H. Herz, *Photogr. Sci. Eng.* **1974**, *18*, 323-335.
- [5] a) U. De Rossi, J. Moll, M. Spieles, G. Bach, S. Dähne, J. Kriwanek, M. Lisk, *J. Prakt. Chem./Chem.-Ztg* **1995**, *337*, 203-208; b) H. von Berlepsch, C. Böttcher, A. Quart, C. Burger, S. Dähne, S. Kirstein, *J. Phys. Chem. B* **2000**, *104*, 5255-5262; c) K. A. Clark, C. W. Cone, D. A. Vanden Bout, *J. Phys. Chem. C* **2013**, *117*, 26473-26481; d) H. von Berlepsch, C. Böttcher, *Langmuir* **2013**, *29*, 4948-4958; e) D. M. Eisele, D. H. Arias, X. Fu, E. A. Bloemsmas, C. P. Steiner, R. A. Jensen, P. Rebentrost, H. Eisele, A. Tokmakoff, S. Lloyd, K. A. Nelson, D. Nicastro, J. Knoester, M. G. Bawendi, *PNAS* **2014**, *111*, E3367-E3375; f) J. Megow, M. I. S. Rohr, M. Schmidt am Busch, T. Renger, R. Mitric, S. Kirstein, J. P. Rabe, V. May, *Phys. Chem. Chem. Phys.* **2015**, *17*, 6741-6747; g) J. R. Caram, S. Doria, D. M. Eisele, F. S. Freyria, T. S. Sinclair, P. Rebentrost, S. Lloyd, M. G. Bawendi, *Nano Lett.* **2016**; h) C. Friedl, T. Renger, H. von Berlepsch, K. Ludwig, M. Schmidt am Busch, J. Megow, *J. Phys. Chem. C* **2016**; i) B. Kriete, A. S. Bondarenko, V. R. Jumde, L. E. Franken, A. J. Minnaard, T. L. C. Jansen, J. Knoester, M. S. Pshenichnikov, *J. Phys. Chem. Lett.* **2017**, 2895-2901; j) W. Cao, E. M. Sletten, *J. Am. Chem. Soc.* **2018**, *140*, 2727-2730; k) S. Doria, T. S. Sinclair, N. D. Klein, D. I. G. Bennett, C. Chuang, F. S. Freyria, C. P. Steiner, P. Foggi, K. A. Nelson, J. S. Cao, A. Aspuru-Guzik, S. Lloyd, J. R. Caram, M. G. Bawendi, *ACS Nano* **2018**, *12*, 4556-4564; l) R. Pandya, R. Y. S. Chen, A. Cheminal, T. Thomas, A. Thampi, A. Tanoh, J. Richter, R. Shivanna, F. Deschler, C. Schnedermann, A. Rao, *J. Phys. Chem. Lett.* **2018**, *9*, 5604-5611.
- [6] H. von Berlepsch, C. Böttcher, in *J-Aggregates, Vol. 2* (Ed.: T. Kobayashi), **2012**, pp. 119-153.
- [7] G. T. Oostergetel, H. van Amerongen, E. J. Boekema, *Photosynth. Res.* **2010**, *104*, 245-255.
- [8] a) J. Lim, D. Paleček, F. Caycedo-Soler, C. N. Lincoln, J. Prior, H. von Berlepsch, S. F. Huelga, M. B. Plenio, D. Zigmantas, J. Hauer, *Nat. Comm.* **2015**; b) F. Milota, V. I. Prokhorenko, T. Mancal, H. von Berlepsch, O. Bixner, H. F. Kauffmann, J. Hauer, *J. Phys. Chem. A* **2013**, *117*, 6007-6014; c) J. Sperling, A. Nemeth, J. Hauer, D. Abramavicius, S. Mukamel, H. F. Kauffmann, F. Milota, *J. Phys. Chem. A* **2010**, *114*, 8179-8189; d) J. Yuen-Zhou, D. H. Arias, D. M. Eisele, C. P. Steiner, J. J. Krich, M. G. Bawendi, K. A. Nelson, A. Aspuru-Guzik, *ACS Nano* **2014**, *8*, 5527-5534; e) B. Kriete, J. Luttig, T. Kunsel, P. Maly, T. L. C. Jansen, J. Knoester, T. Brixner, M. S. Pshenichnikov, *Nat. Comm.* **2019**, *10*.
- [9] a) C. Didraga, A. Pugžlys, P. R. Hania, H. von Berlepsch, K. Duppen, J. Knoester, *J Phys Chem B* **2004**, *108*, 14976-14985; b) A. Eisfeld, R. Kniprath, J. S. Briggs, *J. Chem. Phys.* **2007**, *126*, 104904.
- [10] a) A. Pawlik, S. Kirstein, U. De Rossi, S. Dähne, *J. Phys. Chem. B* **1997**, *101*, 5646-5651; b) A. Pawlik, A. Quart, S. Kirstein, H. W. Abraham, S. Daehne, *Eur. J. Org. Chem.* **2003**, 3065-3080.
- [11] H. von Berlepsch, S. Kirstein, C. Böttcher, *J. Phys. Chem. B* **2003**, *107*, 9646-9654.
- [12] H. Mastroph, K. Reiner, J. Mistol, S. Ernst, D. Keil, L. Hennig, *ChemPhysChem* **2009**, *10*, 835-840.
- [13] H. von Berlepsch, M. Regenbrecht, S. Dähne, S. Kirstein, C. Böttcher, *Langmuir* **2002**, *18*, 2901-2907.

- [14] L. Eggers, K. Kolster, V. Buss, *Chirality* **1997**, *9*, 243-249.
- [15] H. von Berlepsch, K. Ludwig, S. Kirstein, C. Böttcher, *Chem. Phys.* **2011**, *385*, 27-34.
- [16] G. Garab, H. van Amerongen, *Photosynt. Res.* **2009**, *101*, 135-146.
- [17] H. von Berlepsch, C. Böttcher, *Phys. Chem. Chem. Phys.* **2018**, *20*, 18969-18977.
- [18] H. von Berlepsch, S. Kirstein, R. Hania, C. Didraga, A. Pugžlys, C. Böttcher, *J. Phys. Chem. B* **2003**, *107*, 14176-14184.
- [19] H. von Berlepsch, S. Kirstein, R. Hania, A. Pugžlys, C. Böttcher, *J. Phys. Chem. B* **2007**, *111*, 1701-1711.
- [20] AMIRA Software V2019.1 (Thermo Fisher Scientific Inc., Waltham, Massachusetts, USA)
- [21] H. von Berlepsch, S. Kirstein, C. Böttcher, *Langmuir* **2002**, *18*, 7699-7705.
- [22] a) V. Czikkely, H. D. Försterling, H. Kuhn, *Chem. Phys. Lett.* **1970**, *6*, 207-210; b) V. Czikkely, H. D. Försterling, H. Kuhn, *Chem. Phys. Lett.* **1970**, *6*, 11-14.
- [23] D. M. Eisele, C. W. Cone, E. A. Bloemsma, S. M. Vlaming, C. G. F. van der Kwaak, R. J. Silbey, M. G. Bawendi, Knoester, J. P. Rabe, D. A. Vanden Bout, *Nat. Chem.* **2012**, *4*, 655-662.
- [24] M. Liu, L. Zhang, T. Wang, *Chem. Rev.* **2015**, *115*, 7304-7397.
- [25] S. Kumar, K. Ludwig, B. Schade, H. von Berlepsch, I. Papp, R. Tyagi, M. Gulia, R. Haag, C. Böttcher, *Chemistry* **2016**, *22*, 5629-5636.
- [26] R. Marrington, T. R. Dafforn, D. J. Halsall, J. I. MacDonald, M. Hicks, A. Rodger, *Analyst* **2005**, *130*, 1608-1616.
- [27] J. R. Kremer, D. N. Mastronarde, J. R. McIntosh, *J. Struct. Biol.* **1996**, *116*, 71-76.
- [28] G. Tang, L. Peng, P.R. Baldwin, D.S. Mann, W. Jiang, I. Rees, S.J. Ludtke, *J. Struct. Biol.* **2007**, *157*, 38-46.
- [29] J. E. Sader, J. W. M. Chon, P. Mulvaney, *Rev. Sci. Instrum.* **1999**, *70*, 3967-3969.
- [30] B. Foster, *Am. Lab.* **2012**, *44*, 24-28.
- [31] M. Goubert, L. Toupet, M. E. Sinibaldi, I. Canet, *Tetrahedron* **2007**, *63*, 8255-8266.